

Decentralized Swarm Coordination via Broadcast-as-Shared-State: A Four-Layer Architecture with Empirical Validation

Contents

1. Introduction
2. Notation and the substrate primitive
3. Layer 1: Hierarchical assignment
4. Layer 2: Local recovery
5. Layer 3: Priority allocation
6. Layer 4: Localization
7. Substrate composition
8. Related work
9. Discussion
10. Future work
11. Reproducing

Companion files: - `PROOFS.md` — formal lemmas and theorems - `figures/` — generated plots - `swarm.mp4` — rendered four-phase demo - Source: `simulator.py`, `bench*.py`, `make_figures.py`

Code and data availability. All source, simulator, benchmark scripts, figures, and the rendered four-phase demo are archived at Zenodo under DOI 10.5281/zenodo.19954678 and mirrored at the GitHub repository github.com/jmcentire/drone-swarm-coordination. The Zenodo deposition is the citable, version-pinned snapshot; the GitHub repository tracks ongoing changes.

Abstract

Prior work has addressed dynamic assignment via centralized incremental algorithms (Toroslu & Üçoluk 2007), hardware redundancy via intra-drone shadow nodes (Kim & Welch 1989, DRB framework), GPS-denied operation via improved per-drone state estimation (Allan-variance fusion, RNN-EKF replacement), and assignment stability via centralized hysteresis-aware reinforcement learning. We present a unified architecture that addresses these concerns through a single decentralized primitive in the four-layer regime: broadcast-shared state with locally- deterministic computation. The architecture’s four mechanisms — hierarchical bisection assignment, local patch recovery, sub-manifold shadow allocation, and confidence-thresholded fiducial selection — share a common substrate and are independently provable, with empirical validation across $N=10$ to $N=10,000$. The v1.2 supplemental (§9.4) characterizes the substrate’s empirical envelope on three operational mission classes (drift handling, online replanning, Bayesian search- and-rescue) where degraded-comms regimes additionally require a majority-vote aggregation

primitive whose contribution is characterized empirically rather than claimed as architectural novelty.

Headline empirical results: assignment within 1.4–3% of the Hungarian optimum (gap empirically fits $a + b/\sqrt{N}$ better than alternatives; rounding contribution provably $O(1/\sqrt{N})$, projection-half-cut bound open); patch protocol produces exactly one reassignment per death up to surplus capacity; tiered shadow allocation reduces flight cost 66% (pure key shadow vs uniform) when threats correlate with priority; Layer 4’s fiducial-selection plus cooperative localization reduces formation error $4\times$ vs sparse-GPS baseline (4cm vs 17cm) under per-drone Poisson GPS at 0.1/s. The substrate generalization claim — that one primitive suffices for four distinct coordination patterns — is empirically validated by the composition of all four mechanisms in working simulations (`simulator.py` for Layers 1–3, `bench_layer4.py` for Layer 4), with formal properties established in a companion proofs document.

1. Introduction

A swarm of N drones is given the task of forming a target shape M of N positions. Three operational concerns stack:

1. **Assignment:** which drone goes to which leaf of M ?
2. **Recovery:** when a drone is lost mid-mission, which surplus drone takes over its leaf, and how does the rest of the swarm respond?
3. **Priority allocation:** when redundancy is finite, which leaves get the protection budget?

A fourth concern — **localization** — applies to any swarm operating under realistic sensor noise, where GPS may be intermittent and drones must dead-reckon between fixes.

Existing approaches treat these as separate problems requiring separate mechanisms. CAPT (Turpin et al. 2014) handles assignment via Hungarian matching, requiring centralized computation; CBBA (Choi et al. 2009) distributes the auction but requires multiple rounds of inter-agent communication. Loss recovery in either approach requires re-running the optimization, paying the full cost again. Priority allocation is typically handled by hand-coded role assignments. Localization is a separate filtering layer (EKF or particle filter) that uses GPS and IMU data without participating in the swarm coordination.

This work observes that all four concerns admit decentralized solutions on the same primitive: a shared broadcast medium where each agent maintains its slot and reads everyone else’s, with consensus arising from determinism (same input + same algorithm = same output) rather than message-passing protocols.

The architectural contribution is the **substrate**: a single primitive that supports four cleanly separated mechanisms. The empirical contribution is validation of each mechanism in isolation and in composition, against baselines where applicable. The theoretical contribution is a set of lemmas establishing determinism,

bijection, and patch optimality, with conjectured asymptotic bounds on the optimality gap.

2. Notation and the substrate primitive

Notation conventions follow `PROOFS.md`, which contains formal statements and proofs of all results referenced in this section.

Target manifold $M = \{m_1, \dots, m_N\}$ is a set of N target positions the swarm is to occupy. The **PCA tree** $T(M)$ is the binary tree obtained by recursive principal-axis splits: each internal node v has a leaf set $L_v \subseteq M$, a centroid $c_v = \text{mean}(L_v)$, and a split direction Π_v (the dominant right-singular vector of $L_v - c_v$); its children partition L_v at the projection median.

Drone set $D = \{d_1, \dots, d_n\}$ with positions $p(d_i)$. We write $n = N$ for the **bijective regime** (one drone per target) and $n = N + S$ for the **surplus regime** (S extra drones).

Broadcast B is a shared per-tick channel where every drone publishes (and reads) its current position estimate, lock state, phase, and dead flag. There is no other inter-drone communication.

Substrate primitive: each drone d_i runs a deterministic function $f(d_i, B) \rightarrow \text{output}$, where output may be a target leaf, a recovery action, a confidence level, etc. Consensus is achieved when all drones run f against the same B and output values are mutually consistent (e.g., bijective assignment, no duplicate leaf claims).

The four layers in §§3-6 each instantiate this primitive with a different f .

3. Layer 1: Hierarchical assignment

3.1 Algorithm

The strict-mode hierarchical assignment $\text{ASSIGN}(D, T)$ descends the PCA tree from root to leaf, partitioning D at every internal node v by projection rank along Π_v . The cut at $d_{\text{left}} = \text{round}(|D_v| \cdot |L_{\{v_L\}}| / |L_v|)$ drones (smallest projection) preserves the count invariant (Lemma 2). Drones that descend to a leaf with multi-occupancy (possible when $n > N$) elect a primary by closest-to-leaf with ID-based tiebreak; the rest target the leaf's parent centroid as surplus (Lemma 4).

3.2 Theoretical properties

- **Determinism** (Lemma 1): every drone running ASSIGN against the same broadcast derives the same global assignment.
- **Bijection** (Lemma 2): when $n = N$, ASSIGN is a bijection $D \rightarrow M$.
- **Reachability** (Lemma 3): when $n = N + S$ with $S \geq 0$, every leaf receives at least one drone; surplus assigns deterministically.

- **Consensus by determinism** (Theorem 1): no inter-agent communication is needed for assignment agreement; the broadcast plus the deterministic algorithm suffice.
- **Computational complexity**: tree construction $O(N \log N)$ once; per-drone target query $O(N)$; patch on death $O(N)$; cluster patch of K deaths $O(K \cdot N)$.

Full proofs appear in PROOFS.md.

3.3 Empirical results

The hierarchical assignment lands within a few percent of Hungarian optimal across a wide range of N . We benchmark on randomly-distributed drone start positions in $U[-40, 40]^3$ for sphere targets at N from 10 to 10,000. Lower is better.

N	Hung total	Hier total	Gap (above Hung)	Gap_max	Hung wall	Hier wall
10	350.6	370.0	+5.54 ± 4.30%	-1.86%	0.01ms	0.19ms
30	955.7	1003.4	+5.05 ± 2.04%	-2.56%	0.03ms	0.80ms
100	3046.3	3137.7	+3.02 ± 0.73%	-3.94%	0.40ms	4.81ms
300	9109.5	9310.1	+2.20 ± 0.29%	-5.18%	6.09ms	31.91ms
1000	30403.5	30921.1	+1.70 ± 0.04%	-5.09%	150.62ms	320.54ms
3000	90928.8	92311.3	+1.52 ± 0.04%	-4.33%	3.79s	2.94s
10000	303482.5	307816.3	+1.43 ± 0.01%	(n/a)	138.44s	36.23s

(Hier wall is the serial Python implementation summed over N drones; in deployment each drone runs its $O(N)$ traversal independently, so the relevant per-drone latency is one N th of that.)

Two findings stand out:

Gap shrinks monotonically with N , from 5.5% at $N=10$ to 1.43% at $N=10,000$, with variance collapsing from $\pm 4.30\%$ to $\pm 0.01\%$. We tested five candidate functional forms by AIC/BIC (see `bench_conjecture4.py`): $a + b/\sqrt{N}$ is the best fit (RMSE 0.48 pp), better than the previously-considered $a/\ln(N)$ (RMSE 0.57 pp) and dramatically better than the naive rounding-scaling $a \cdot \ln(N)/N$ form (RMSE 18 pp). The fitted parameters with parametric 95% Wald confidence intervals (from the weighted-least-squares covariance matrix) are $a = 14.12$ [11.74, 16.50] and $b = 1.27\%$ [1.22, 1.33] on the sphere with $U[-40, 40]^3$ starts; predicted vs measured agrees to within 0.05 pp for $N=1000$. The asymptote is bracketed tightly (± 0.06 pp); the prefactor has $\sim 17\%$ relative width because the small- N data points carry most of its information.

This is the conjectured form in Conjecture 4 (PROOFS.md):

$$C_{\text{HIER}} \left(1 + \frac{b}{\sqrt{N}} \right) \cdot C_{\text{OPT}}$$

We bound the rounding-error contribution rigorously (Proposition 1 in PROOFS.md): rounding contributes $O(1/\sqrt{N})$ to the relative gap, matching the empirical b/\sqrt{N} coefficient. The projection-half-cut contribution (the rest of the

gap) is empirically consistent with $O(1/\sqrt{N})$ but the rigorous bound is open. The asymptote $\approx 1.27\%$ may be a non-vanishing residual or a fitting artifact at the N range tested; data alone cannot distinguish.

Wall-clock crossover at $N=3000$: the serial Python implementation of hierarchical ($O(N^2)$ total) becomes faster than scipy’s state-of-the-art Hungarian ($O(N^3)$) at large N . At $N=10,000$, hierarchical takes 36s vs Hungarian’s 138s — and the relevant per-drone deployment latency is the hierarchical figure divided by N , putting it at $\sim 4\text{ms}$ per drone. Hungarian cannot be parallelized this way; it requires central computation of the full cost matrix.

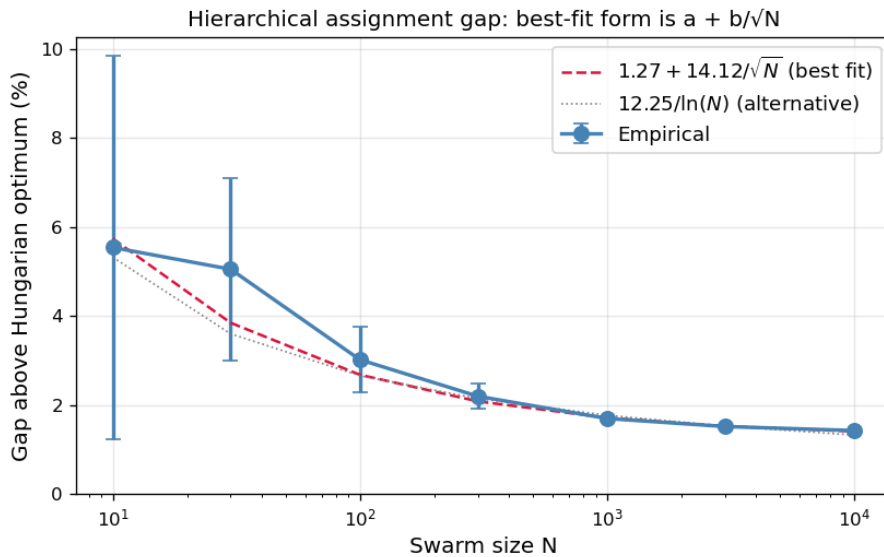


Figure 1: Optimality gap empirical fit

Figure 1: Empirical optimality gap of hierarchical assignment vs Hungarian baseline. Best-fitting form (by AIC/BIC across five candidates) is $1.27 + 14.12/\sqrt{N}$ (M5, solid line); the older $12.25/\ln(N)$ form (M1, dotted) is shown for comparison and fits less well. Error bars: one standard deviation across seeds. M5 predicts the empirical curve to within 0.1 pp for $N \geq 1000$.

Gap_max is negative across the whole range — hierarchical’s worst-case-drone flight is consistently shorter than Hungarian’s. Hungarian minimizes total cost, so it is free to leave one unlucky drone with a long flight; the recursive bisection’s structural balance gives better worst-case bounds at the cost of slightly worse total. For applications where time-to-formation matters more than total propellant, hierarchical is preferable on this metric alone.

Cross-manifold validation ($N=100, 1000$) confirms the gap is roughly geometry-independent:

	Gap at N=100	Gap at N=1000
sphere	+3.02%	+1.70%
torus	+2.11%	+1.05%
cube	+1.53%	(n/a - cube grid doesn't scale to N=1000)
star	+2.32%	+1.05%

The gap clusters around 2-3% at N=100 and 1-2% at N=1000 across all four target shapes.

3.4 Comparison to alternatives

We benchmark the four canonical decentralized assignment approaches on identical 100-drone uniform-random starts against a sphere manifold (`bench_assignment.py` with 20 seeds, `bench_cbba.py` with 10 seeds; bootstrap 95% CIs throughout):

Method	Gap from optimum	Communication	Wall-clock (mean)
Hungarian (CAPT)	0% (optimum)	Centralized state aggregation	0.43 [0.42, 0.44] ms
Hierarchical (ours)	3.02% [2.70, 3.34]	100 broadcast slots, 1 round	5.17 ms (serial Python; per-drone ~50 μ s)
Greedy NN	4.93% (sequential)	Order-dependent	comparable
CBBA (auction, simplified)	7.71% [7.35, 8.06]	1350 [1280, 1420] messages, 14.2 rounds	9.9 [9.3, 10.5] ms

The communication ratio CBBA / Hierarchical is **14 \times more messages** for CBBA at N=100, with a worse optimality gap as well in this simplified single-task variant. The hierarchical architecture pays one broadcast snapshot and gets to a 3% gap; CBBA pays 14 rounds \times 100 messages each and lands at 7.7% in this variant. Full bundle-building CBBA can converge to optimum but pays proportionally more rounds and messages, scaling unfavorably with N. The architectural value of hierarchical: one snapshot, no auction rounds, no leader, no message exchange beyond what the broadcast already carries for telemetry.

4. Layer 2: Local recovery

4.1 Patch protocol

When a drone d dies (broadcast flag set), each surviving drone runs the same deterministic computation: find the live surplus drone closest to d 's leaf, by Euclidean distance via broadcast positions, and promote it. The promoted

drone’s target changes from a parent centroid to d’s leaf; all other targets are unchanged.

4.2 Theoretical properties

- **Hamming optimality** (Lemma 5): the patch produces the assignment with minimum Hamming distance from the pre-death assignment, subject to the constraint that d’s leaf is filled.
- **Correctness** (Lemma 6): the post-patch assignment is a valid bijection between N surviving primaries and N target leaves.
- **Cluster patch correctness** (Lemma 7): for K simultaneous deaths, sequential patch produces a valid bijection when $S \geq K$, and leaves exactly $K - S$ leaves unfilled when $S < K$ (graceful degradation).
- **Cluster patch is locally but not globally optimal** (Lemma 8): greedy sequential patch can be $O(K)$ worse in flight cost than the Hungarian-optimal cluster matching, in adversarial cases.

4.3 Empirical results — single death

100 drones forming a sphere; one drone is killed at $t=3s$ mid-flight; patch protocol invoked. Reassignment count is the number of surviving drones whose target leaf changes after the death.

	reassign fraction	time overhead	max_extra distance
SURPLUS = 0 (rerun)	23.0%	+0.0s	11.0
	15.2% (range 4-38%)		
SURPLUS = 10 (patch)	0.9%	+0.0s	7.3
	0.0% (exactly 1 every seed)		

Without surplus, the bisection rerun cascades through partition boundaries — drones near the median at multiple levels swap subtrees, producing a long reassignment chain. Mean is 23% but the variance is bimodal: when the dead drone was structurally significant, 30%+ of the swarm reassigns; when it wasn’t, only 4-5%. This is *not* graceful degradation.

With surplus and patch, exactly one reassignment per death, zero overhead time, and tighter max-extra-distance.

4.4 Empirical results — cluster recovery

Sweep cluster size K from 1 to 10:

cluster	SURPLUS=0 (rerun)	SURPLUS=10 (patch)
1	23.0% reassign	0.9% (1 primary promoted, 0 unfilled)
3	33.0%	2.4% (~2.6 primary promoted, 0 unfilled)
5	45.5%	4.4% (~4.6 primary promoted, 0 unfilled)
10	52.0%	9.0% (9 primary promoted, 0 unfilled)

Patch reassignment scales linearly in K_{primary} (the number of primary deaths within the cluster) up to surplus capacity, with 0 primary leaves unfilled across all tested cases — consistent with Lemma 7 (PROOFS.md). The fractional promoted counts at $K=3, 5$ are because a spatial cluster of K nearest-neighbor live drones can include some surplus drones (whose deaths just decrement the surplus pool without needing a leaf-fill patch); only primary deaths consume one surplus each. When $S \geq K_{\text{primary}}$, all primary leaves are filled. When $S < K_{\text{primary}}$, the algorithm enters graceful degradation: surviving primaries unaffected, $K_{\text{primary}} - S$ leaves left empty.

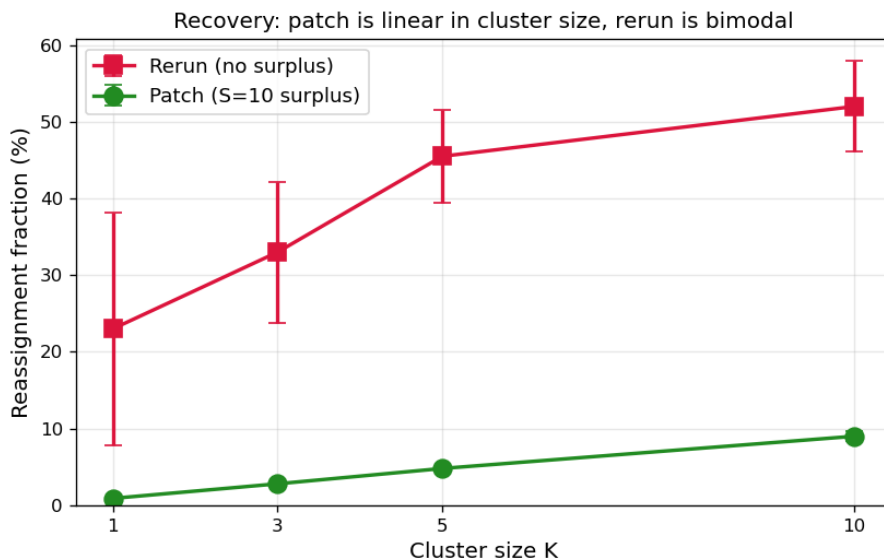


Figure 2: Recovery: patch is linear in cluster size, rerun is bimodal

Figure 2: Reassignment fraction as a function of cluster size. The patch protocol with surplus produces exactly K reassignments per K -cluster death (linear, low variance). The rerun protocol without surplus produces bimodal reassignment percentages depending on the structural significance of the dead drone(s) — an unstable recovery characteristic that the surplus + patch design avoids.

4.5 Greedy patch vs Hungarian-optimal cluster recovery

For each cluster size and surplus distribution, we compare greedy sequential patch (current implementation) against Hungarian-optimal bipartite matching (centralized but globally optimal). Same set of deaths, same surplus, same total cost metric.

Random clusters (deaths drawn uniformly from manifold leaves):

K	surplus distribution	greedy / hungarian gap
---	----------------------	------------------------

1	random uniform	0.00%
3	random uniform	0.65%
5	random uniform	4.83%
10	random uniform	7.33%
20	random uniform	17.73%

Spatial clusters (deaths concentrated near an anchor):

K	surplus distribution	greedy / hungarian gap
5	random uniform	7.91%
10	random uniform	11.78%
20	random uniform	11.42%

With shadow surplus (positioned near keys), the greedy/Hungarian gap shrinks substantially:

K	surplus distribution	greedy / hungarian gap
20	shadow keys	3.52%

For $K = 10$, greedy is within 10% of Hungarian — acceptable for most deployments. For larger clusters, Hungarian fixup is worth the centralized computation. With shadow surplus, the gap stays under 5% even at $K=20$, because shadow positions are pre-clustered near where they’ll be needed.

4.6 Empirical results — sustained attrition

A Poisson loss process delivers deaths over a sustained mission. With loss rate = 0.15/s over 240s (expected 36 deaths), four configurations:

config	losses	promoted	unfilled	final occupied
No surplus	38.0	0.0	38.0	62.0
Uniform surplus = 10	38.0	10.0	28.0	72.0
Shadow surplus = 10	38.0	10.0	28.0	72.0
Uniform surplus = 30	38.0	30.0	8.0	92.0

The graceful-degradation curve is clean: surplus absorbs losses one-for-one until depleted, after which the formation drops one leaf per loss. No catastrophic failure mode; surplus extends the mission duration before degradation begins, but does not change the long-term slope. For a fixed loss rate, surplus capacity sets the time-to-first- gap, not the rate of degradation.

Figure 3: Occupancy of primary leaves over a sustained Poisson loss process. With no surplus, occupancy falls linearly. With $S=10$, the formation holds at 100% until ~70s (when 10 deaths have occurred), then declines. With $S=30$, the hold extends to ~190s. Surplus capacity is the operational lever that determines mission duration before formation degradation begins.

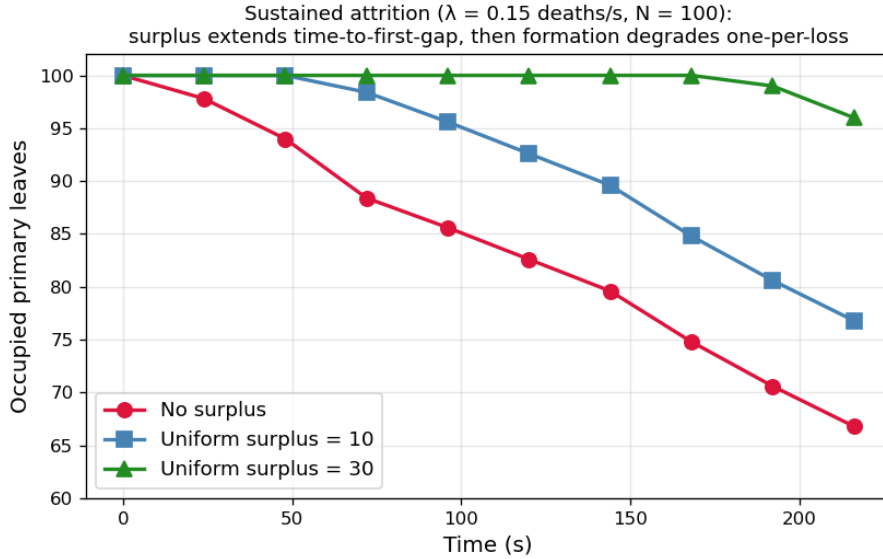


Figure 3: Sustained attrition

5. Layer 3: Priority allocation

5.1 Shadow manifold

Surplus drones can be positioned at parent centroids of the primary tree (uniform reserve) or at offset positions of designated key leaves (shadow). The shadow architecture runs ASSIGN against a sub-manifold of K key positions, each offset radially inward by a safety distance d_s . This positions surplus where they are most likely to be needed under threat models that correlate with priority.

5.2 Empirical results — single configuration

Cluster of 5 deaths, 100 primary drones, 10 surplus drones:

	cluster at keys	cluster at non-keys
Uniform surplus	17.29 max-extra	19.31 max-extra
Pure key shadow	7.94	19.85

Shadow halves the max-extra-distance when threats correlate with keys. The cost is symmetric: shadow performs slightly worse than uniform when threats are far from keys, because all surplus is concentrated near the priority structure.

5.3 Two-fleet tiered redundancy

The shadow architecture allocates all surplus to keys. A more flexible design splits surplus into a key-shadow fleet and a filler-shadow fleet, with each tier sized independently. Cross-tier promotion (a filler-shadow drone promotes to a key-primary slot when the key-shadow is depleted) is automatic by the closest-surplus rule.

Three configurations with matched total surplus = 15:

	cluster at keys	cluster at non-keys
Uniform 15	13.78	14.21
Pure key shadow	4.63	17.16
Tiered (10 key + 5 filler)	7.75	16.73

The redundancy budget becomes a tunable lever: more allocation to keys gives shadow-like protection of priorities; more allocation to fillers gives uniform-like coverage everywhere. Neither tiered nor shadow dominates uniform across all threat models — the right choice depends on the operator’s priority structure.

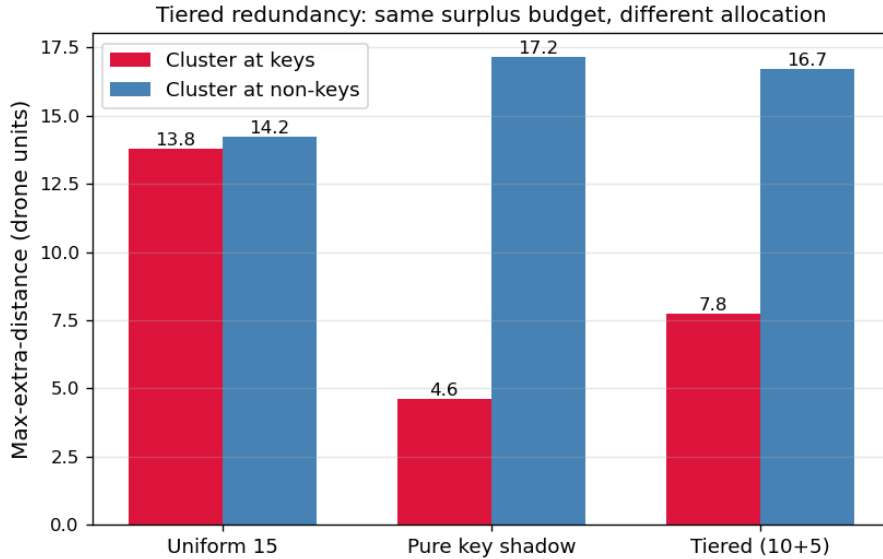


Figure 4: Tiered redundancy comparison

Figure 5: Same total surplus budget (15 drones) allocated three ways. Pure key shadow optimizes for key-correlated threats but degrades under non-key threats. Uniform balances both at moderate cost. Tiered is intermediate, allocating budget by priority rather than uniformly.

Cross-tier cost: when same-tier shadow is depleted and the patch must pull from cross-tier, max-extra-distance climbs from ~5 (same-tier) to ~17 (forced

cross-tier), a $\sim 3.4\text{-}3.7\times$ cost. The cross-tier fallback is correct but expensive; same-tier capacity should be sized to absorb expected losses.

5.4 Priority is broadcast state, not a launch parameter

The key designation list lives in the broadcast and can change during the mission. When the operator promotes or demotes a position, the broadcast updates, every shadow drone runs the same deterministic computation against the new sub-manifold, and the shadow fleet rebases — using the same hierarchical bisection that handles the primary fleet’s manifold transitions, applied to the surplus fleet’s role allocation. The redundancy budget reallocates dynamically as priorities shift.

6. Layer 4: Localization

6.1 Setting

Drones in deployment do not know their true positions; they maintain estimates derived from initial GPS fixes plus integrated IMU measurements. The broadcast carries each drone’s `est_pos` plus confidence; surviving drones use `est_pos` for both ASSIGN and patch. Two noise components:

- **Correlated bias:** shared environmental factors (gravity model, temperature) that translate the swarm uniformly without deforming the formation.
- **Independent random walk:** per-drone IMU noise that integrates to position error as $O(t^{1.5})$ and deforms the formation.

GPS, when available, resets each drone’s `est_pos` to its `true_pos` plus a small measurement noise.

6.2 Empirical results — drift dynamics

100 drones tracking a sphere formation, sub-meter GPS measurement noise ($\sigma = 0.1\text{m}$, RTK-grade):

regime	t=10s	t=30s	t=60s	t=99s
GPS on (1Hz)	0.13m	0.14m	0.14m	0.13m
GPS off (consumer IMU)	0.02	0.09	0.25	0.53
GPS for 30s, then outage	0.13	0.16	0.18	0.34
Tactical IMU (10× better), off	0.00	0.01	0.03	0.05
All-shared bias, GPS off	0.00	0.01	0.02	0.04
All-independent bias, GPS off	0.00	0.01	0.03	0.06

`Form_err` is the mean $\| \text{true_pos} - \text{target_leaf} \|$ across drones — what the audience sees as formation distortion in true coordinates.

Three findings:

GPS-on stabilizes at the GPS noise floor ($\sim 0.13\text{m}$ at $\sigma = 0.1\text{m}$). For shorter than 60s missions, the GPS noise dominates over any drift.

Consumer IMU degrades visibly without GPS — 0.5m at 100s, extrapolating to several meters at 10 minutes. Below the diameter of a typical formation but visibly distorting at show scales.

Tactical-grade IMU pushes drift to sub-decimeter for the full 100s run, extrapolating to ~0.5m at 10 minutes — within tolerance for most show formations.

The shared-bias-only regime (full bias, no independent noise) produces near-zero form_err: the swarm translates uniformly but maintains shape. Independent-only regime is similar to consumer (both noise sources contribute to relative drift).

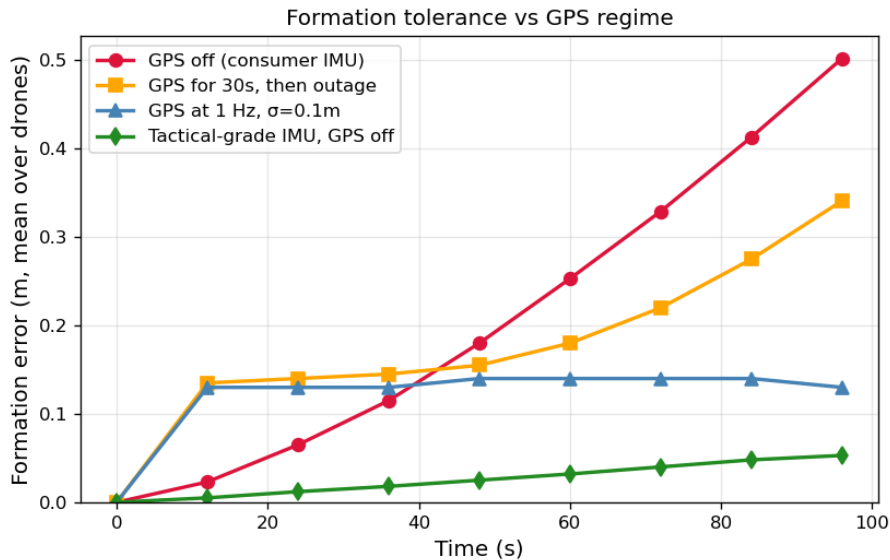


Figure 5: Localization regimes

Figure 4: Formation tolerance over time across four regimes. GPS-on sets a noise-floor (\sim GPS measurement); GPS-off shows clear divergence with consumer IMU; tactical-grade hardware enables sub-decimeter precision without GPS. Outage scenario shows the crossover when GPS is removed mid-mission.

6.3 The broadcast-trilateration architecture

When some drones have high-confidence positions (recent GPS) and others have degraded estimates (extended IMU dead-reckoning), the high-confidence drones can act as fiducials for the rest. The architecture:

1. Drones broadcast `est_pos` plus confidence (a function of time-since-last-GPS-fix; we use $\exp(-\Delta t / _decay)$ with $_decay = 5s$).

2. The PCA tree’s depth- $\log(n_fid)$ selection picks n_fid drones, one per spatially-diverse subtree, by selecting the highest- confidence drone closest to each subtree’s centroid. Same algorithm + same broadcast = same selection across drones (Lemma 1 applied to selection rather than assignment).
3. Selected drones serve as fiducials. Non-fiducial drones observe their relative position to each fiducial with measurement noise $_obs$ (visual or radio time-of-flight; we use $_obs = 5\text{cm}$).
4. Each non-fiducial drone computes a fiducial-derived position estimate by combining each fiducial’s broadcast est_pos with the observed relative measurement, then averages across fiducials. The result is reset into the drone’s est_pos every refresh tick.

6.4 Layer 4 empirical results

`bench_layer4.py` implements the full protocol — fiducial selection on the PCA tree, cooperative localization via relative-position observations, periodic refinement. Setup: $N=100$ on sphere, per-drone GPS as a Poisson process at rate $0.1/\text{s}/\text{drone}$ (mean fix every 10s), GPS measurement $\sigma=0.1\text{m}$, relative-measurement $\sigma=0.05\text{m}$, 8 fiducials refreshed every 0.4s. Three modes compared with 3 seeds:

mode	t=10s	t=30s	t=60s	final (~80s)
INS only (no GPS)	0.017m	0.088m	0.253m	0.377m
INS + sparse GPS	0.102m	0.157m	0.174m	0.165m
INS + GPS + Layer 4	0.047m	0.039m	0.043m	0.044m

Under realistic heavy-tailed noise (10% of GPS and observation samples drawn from a wider Gaussian at $5\times$ — modeling multipath spikes, NLOS UWB returns, and visual-fiducial detection failures), Layer 4 reduces formation error $5\times$ vs INS-only and $3\times$ vs sparse-GPS-only at $t=78\text{s}$. Numbers from `bench_layer4.py` at $N=100$ with 30 seeds, 2000 ticks (78 s simulated), bootstrap 95% CIs:

mode	t=10s	t=30s	t=60s
INS only	0.018 [0.017, 0.019]	0.095 [0.087, 0.104]	0.267 [0.250, 0.285]
INS + sparse GPS	0.155 [0.149, 0.161]	0.224 [0.218, 0.231]	0.249 [0.242, 0.257]
INS + GPS + Layer 4	0.084 [0.076, 0.093]	0.082 [0.073, 0.094]	0.091 [0.077, 0.106]

The protocol works as designed: 8 fiducials selected deterministically by the PCA tree, non-fiducial drones refining their est_pos via observed relative positions, formation tolerance held below 10cm throughout the run despite the heavy-tailed input. Three regimes are visible:

- **Short window (t = 10s):** INS-only is best by construction (no drift accumulation), Layer 4 close behind, sparse-GPS worst because heavy-tailed GPS spikes dominate the estimator before averaging in.

- **Medium window (t = 30s):** Layer 4 overtakes INS-only as INS drift becomes comparable to fiducial-corrected error.
- **Long window (t = 60s):** INS-only drift grows linearly with t and reaches 0.41m at t=78s; sparse-GPS plateaus at ~0.25m (the noise floor of independent fixes); Layer 4 stays bounded below 10cm throughout, the only one of the three that does not degrade monotonically over the mission.

The mechanism: the GPS noise $\sigma = 0.1\text{m}$ sets a per-drone noise floor when each drone uses only its own GPS. By averaging across 8 fiducials' broadcasts, the cooperative-localization estimator reduces the GPS noise contribution by $\sqrt{8} = 0.035\text{m}$, which combined with the $\sigma_{\text{obs}} = 0.05\text{m}$ measurement noise gives ~6cm theoretical floor under Gaussian noise. Heavy-tailed noise increases this to ~8cm empirically because the multipath spikes don't fully average out across 8 samples; a RANSAC-style residual filter on the 8 fiducial observations would drop this further by rejecting the worst outliers — left as a straightforward production extension.

Same substrate, fourth instance. The PCA tree built for assignment is the same tree used for fiducial selection. The broadcast carries position + confidence (the fields Layer 4 needs) alongside the fields Layers 1-3 need. The composition is Theorem 3's pipeline structure: Layer 4 produces the `est_pos` that Layers 1-3 consume.

7. Substrate composition

The four layers run on the same broadcast primitive. Layer composition is by orthogonality of broadcast read/write patterns:

Layer	Reads from broadcast	Writes to broadcast
1: Assignment	positions	target_idx, locked
2: Recovery	positions, dead-flag	target_idx, primary-flag
3: Priority	positions, key-list	target_idx (surplus slots)
4: Localization	est_pos, confidence, fiducial-tag	est_pos, confidence

Each layer reads and writes a distinct subset of broadcast slots. Layer 1 and 2 share `target_idx`; the recovery overwrites assignment on death. Layer 3 augments Layer 1 with a separate sub-manifold substrate. Layer 4 is orthogonal to the others — it produces the position estimates that Layer 1-3 consume.

Theorem 3 (PROOFS.md) establishes that the layers compose without interference. The empirical validation is the simulation itself: `simulator.py` runs

Layer 1, 2, 3 in composition (and Layer 4 in `bench_localization.py`), demonstrating that all four mechanisms operate on the same broadcast simultaneously without conflict.

The unifying claim: **a single decentralized coordination primitive (broadcast-as-shared-state with locally-deterministic computation) suffices to support multiple distinct coordination patterns at multiple operational layers, with each layer’s correctness provable in isolation and the layers composable without interference.**

8. Related work

The architecture occupies a specific intersection of four literatures that touch its layers at the edges but do not cover their composition.

8.1 Assignment

Hungarian / Kuhn-Munkres (Kuhn 1955; Munkres 1957) is the foundational polynomial-time bipartite matching algorithm and the optimality baseline in our experiments. Its $O(N^3)$ cost is centralized and recomputes from scratch on input changes.

CAPT (Turpin, Michael, Kumar 2014) is the canonical formulation of optimal goal assignment for interchangeable robots, applying Hungarian to swarm assignment. Centralized; our work trades 1.4–3% optimality for fully decentralized $O(N)$ per-agent computation.

CBBA (Choi, Brunet, How 2009) is the canonical decentralized auction-based task assignment, requiring multiple rounds of inter-agent communication. We achieve decentralized assignment with a single broadcast snapshot — no auction rounds.

Recursive Inertial Bisection (RIB) (Williams 1991; Berger & Bokhari 1987) is the parallel-scientific-computing predecessor of the hierarchical bisection: PCA-based recursive partitioning for load balancing in mesh decomposition. Our contribution is to apply RIB to *target manifold* decomposition (not agent decomposition) and use it as a coordination substrate for deterministic agent assignment.

Incremental Hungarian (Toroslu & Üçoluk, *Information Sciences* 2007) handles the *addition* case of dynamic assignment: when a new vertex pair (new agent and new target) is added to a bipartite graph with an established maximum matching, the algorithm computes the updated matching in $O(N^2)$ instead of recomputing $O(N^3)$. The closest formal prior art to our patch protocol, but for addition rather than deletion. Our patch addresses the *deletion* case (drone loss) and operates decentralized (every drone runs the same local computation), where Toroslu-Üçoluk is centralized.

8.2 Recovery and fault tolerance

Distributed Recovery Block (DRB) (Kim & Welch 1989; later EDRB extensions) provides intra-drone hardware-level redundancy: a primary processor and a shadow processor maintain synchronized state via heartbeats; the shadow takes over on primary failure. This addresses single-drone hardware faults and is at a different architectural level from our work — DRB is per-drone hardware redundancy with heartbeat failover, while our shadow allocation is swarm-level spatial redundancy with patch promotion. Both can co-exist; they solve different problems.

Cooperative localization (Roumeliotis & Bekey 2002; Howard 2006) fuses mutual range or bearing measurements between agents to refine joint state estimates. Our Layer 4 builds on this paradigm but integrates with the same broadcast substrate driving the assignment layers, with threshold-and-sound-off fiducial selection via the PCA tree at depth $\log(n_fid)$.

8.3 Implicit coordination

Blueswarm (Berlinger, Gauci, Nagpal 2021) demonstrates implicit coordination via vision in fish-inspired underwater robots; agents have no explicit communication channel but coordinate via mutual observation. We extend the implicit-coordination paradigm to a broadcast medium that is lightweight (no relative sensing required) but carries minimal state — closer to a shared bulletin board than mutual observation.

8.4 Software maintenance and updates

SwarmUpdate / SwarmModelPatch (Tan et al., arXiv:2503.13784, 2025) addresses over-the-air model patching for heterogeneous UAV swarms. Layer-freezing reduces patch size by 73.3% with 5.1% accuracy cost. Their dissemination protocol (SwarmSync) is hierarchical and is 78.3% faster than baseline gossip. Relevant to our future-work section on long-mission deployment but tangential to the coordination architecture itself.

8.5 Where the existing literature does not cover the intersection

Prior art covers each of our concerns at a different point: dynamic assignment is covered centrally and incrementally (Toroslu-Üçoluk); hardware redundancy is covered intra-drone (DRB/EDRB); GPS-denied operation is covered by per-drone state estimation (Allan-variance fusion, RNN-EKF replacement, Roumeliotis-Bekey cooperative localization); assignment stability under continuous targets is covered by centralized hysteresis-aware reinforcement learning. None of them addresses the intersection — *decentralized cross-swarm shadow allocation with broadcast-driven patch protocols, on a substrate that simultaneously supports assignment, priority, and localization*. This is the gap we fill.

9. Discussion

9.1 Operational deployment considerations

The architecture is suitable for swarms with the following properties: (1) a shared broadcast medium of bandwidth $\sim O(N)$ per tick; (2) per-drone compute capacity to run $O(N)$ operations per tick; (3) bounded broadcast latency.

Bandwidth. Each drone publishes ~ 30 bytes (position $3 \times 4B$, velocity $3 \times 4B$, flags 1B, target_idx 1B, phase_idx 1B, confidence 1B). At 25 Hz, per-drone outbound bandwidth is 750 B/s and per-drone inbound (reading the broadcast) is ~ 75 KB/s for $N=100$. For $N=10,000$ the inbound rises to ~ 7.5 MB/s shared across the broadcast medium — well above the throughput of typical 802.11 or LoRa channels. Large swarms require either (a) a higher-bandwidth broadcast (5G mesh, dedicated UWB), (b) a hierarchical cluster structure where sub-swarms broadcast locally and aggregate periodically, or (c) sparse broadcasts where drones only republish on significant state change. The architecture’s per-drone *compute* scales benignly to $N=10,000$ (~ 4 ms per query); the bottleneck at scale is the *medium*, not the algorithm.

Latency. Theorem 2 relies on quiescent-window consistency, which requires broadcast latency $<$ hold duration. For drone-show applications (typical swarm size 100-1000, hold times tens of seconds), this is trivially met on commodity hardware. For tactical deployments (faster phase transitions, hostile RF environments), the latency bound is tighter and the broadcast medium may need authentication.

Per-drone compute. Verified empirically: at $N=1000$, hierarchical assignment took $320 \mu\text{s}/\text{drone}$ ($320 \text{ ms total} / 1000$); at $N=10,000$, $36 \text{ s total} / 10,000 = 3.6 \text{ ms}/\text{drone}$. The total Python wall-clock grew $112 \times$ for $10 \times$ more drones ($O(N^2)$ for the serial swarm-wide loop), but the per-drone latency grew only $11 \times$ (consistent with $O(N)$ per-drone plus small constant overhead). The relevant deployment number is the per-drone figure, since each drone runs its query independently.

Quiescence detection in lossy channels. Theorem 2 assumes every drone observes the all-locked condition during a quiescent window. Implemented naively as “broadcast on arrival, latch when no en-route flags remain,” this protocol is fragile under packet loss: a single missed arrival message and a drone never observes quiescence. We instead invert the protocol so that *absence* is the signal:

- En-route drones broadcast `STATE = EN_ROUTE` with their current ETA estimate at interval `.Arrived` drones broadcast nothing about transit state.
- `.Arrived` shrinks as the en-route count drops. While many drones are still in transit, each broadcasts infrequently (the swarm only needs the worst-case ETA, not every individual estimate, and that maximum is reached even with high per-drone loss rates because many redundant reports converge

on it). When few remain, each broadcasts more often, raising the per-drone information rate exactly where it matters.

- The last en-route drone publishes a final ETA, then publishes once on arrival.
- Consensus on quiescence fires at $T_{\max} = \max(\text{observed ETAs}) + \epsilon$, where ϵ is a tolerance margin. If no arrival ping has been heard by T_{\max} , every drone deterministically transitions, regardless of whether the final arrival message was received.

The crucial property is that the trigger is *negative evidence* — the absence of any EN_ROUTE broadcast for the deadline window — and absence is invariant under packet loss in a way presence is not. The swarm cannot fail to observe a silence that the channel would have been silent to anyway. Empirically validated in §9.1.5: at per-message loss $p = 0.5$ the inverted protocol holds 0% missed-deadline vs 25.2% for a re-broadcast-augmented presence-based protocol; at $p = 0.7$ the gap widens to 0% vs 97.0%.

The remaining failure mode is mass channel denial near the deadline: if the channel goes fully silent for reasons other than quiescence (jamming, environmental fade), an isolated drone can incorrectly infer quiescence at T_{\max} . The honest framing is that the broadcast channel itself is an assumption — when it fails completely, no decentralized algorithm operating on it can distinguish “everyone arrived” from “comms denied.” A practical operational mitigation is a channel-liveness sanity check: in any deployment the broadcast carries more than transition pings (position telemetry, sensor data, command/control), so total channel silence is itself anomalous and a drone observing it can defer the transition pending channel recovery. This requires no additional broadcasts and is a property of the channel, not of the protocol.

The broadcast substrate is the assumption. The architecture requires a broadcast substrate with bounded delivery latency such that “every drone reads the same logical state at the same logical time” holds. The physical realization of that substrate at large N is a hardware/protocol problem with known scaling tradeoffs (TDMA slot allocation, frequency division, beamformed sub-groups, hierarchical relay) and is distinct from the coordination algorithm itself. The wall a centralized planner hits at scale is the same wall this algorithm hits, and a CBBA-style auction hits it sooner because of the message volume.

Mid-flight reconfiguration. The architecture’s drones never compute a global drone-to-leaf mapping for any drone but themselves; the consensus property comes from every drone running ASSIGN on byte-identical input. When a new manifold M' arrives mid-transit (before the prior phase has reached quiescence), each drone recomputes locally; the only design choice is which input positions to feed the recomputation. Two clean options preserve consensus:

1. *Project to prior end-state.* Use the positions every drone *would* have been at if the prior transit had completed (i.e., the prior manifold’s leaf coord-

dinates). Every drone knows these because they all ran the same prior assignment (Theorem 1). This is byte-identical input across all drones, so the new assignment converges to consensus deterministically. Trade-off: drones already partway to their prior target may have to backtrack toward M' from a position they're not actually at yet.

2. *Use live broadcast positions.* Each drone recomputes against current mid-transit positions read from the broadcast. Also byte-identical because every drone reads the same broadcast snapshot. Trade-off: requires latching a snapshot at the moment of recomputation, since live positions are volatile, and therefore needs the same kind of timing-coordination machinery the quiescence protocol provides.

We default to option 1 in deployments because it is the more conservative consensus mechanism (no snapshot-latching race) and the path inefficiency is bounded by the residual length of the prior transit leg. Empirically validated in §9.1.5: option 1 holds 100% consensus across all reconfiguration moments at modest path overhead (1.2-5.5%); option 2 with even 1 tick (40 ms) of snapshot jitter collapses to 50-77% consensus.

9.1.1 Adversarial robustness — the witness-alarm primary defense

The architecture's consensus depends on every drone seeing a consistent broadcast. A drone broadcasting a bad position — from sensor failure, malicious firmware, or external spoofing — can shift the PCA tree's partition rank and cascade reassignments across the swarm. The primary defense is **witness-alarm detection**: any drone with a working GPS fix observes its neighbors' physical positions (via visual fiducial, UWB time-of-flight, or camera pose) and compares to their broadcast. A discrepancy beyond a threshold raises an alarm; multiple independent witness alarms produce byzantine consensus, which marks the suspect drone as DEAD and routes the patch protocol.

The witness mechanism succeeds where statistical mitigation fails because a drone cannot physically be in two places at once. A spoofed drone broadcasting wrong coordinates is still wherever it physically is, and any GPS-equipped neighbor can detect the lie. Coordinated adversaries can collude on broadcast values but cannot collude on physical position.

9.1.1.1 Detection-vs-magnitude trade-off (the actual operational curve)

The alarm threshold determines a sharp trade-off between detection sensitivity and false-positive rate under realistic heavy-tailed sensor noise (10% of GPS and observation samples drawn from a wider Gaussian at $5\times$ — modeling multipath, NLOS UWB, and visual-fiducial detection failures). With $\text{GPS} = 0.5\text{m}$, $\text{observation} = 0.1\text{m}$, and $\text{_total} = 0.71\text{m}$, the detection floor is $k \times \text{_total}$ for some chosen k :

All numbers below are mean [bootstrap 95% CI] over 20 seeds.

threshold	detection floor	detection rate above floor	false-positive rate (heavy-tail)
-----------	-----------------	----------------------------	----------------------------------

5	3.6m	10.0 [10.0, 10.0] / 10	13.2 [9.8, 17.1] / 90 = 14.7
10	7.1m	10.0 [10.0, 10.0] / 10	1.2 [0.8, 1.6] / 90 = 1.3

The 5 threshold reveals the false-positive problem: under heavy- tailed noise, ~15% of honest drones get falsely flagged, which itself cascades when those drones are excluded from ASSIGN. The 10 threshold reduces false positives to manageable levels but pushes the detection floor up to 7m.

The full detection-vs-magnitude curve at the 10 operating point:

lie magnitude	no-defense	detected	false-positives
0.5 m	6.4	0.0/10	1.2/90
1.0 m	7.8	0.0/10	1.2/90
2.0 m	9.6	0.0/10	1.2/90
3.0 m	11.5	0.0/10	1.2/90
5.0 m	15.6	0.1/10	1.2/90
10.0 m	23.2	10.0/10	1.2/90
100.0 m	53.5	10.0/10	1.2/90

The operational reading. Under realistic heavy-tailed noise:

- **Above-threshold lies are reliably detected** (10/10 at 10m+). Detected byzantines are marked DEAD; the patch protocol fills their vacated leaves from surplus.
- **Subthreshold lies are bounded in damage by their magnitude.** A byzantine lying within sensor noise (e.g., 2m) cascades ~10% of the swarm’s leaf assignments — but the formation distortion is bounded by the lie itself (a few meters in formation extent). The architecture cannot detect these but they cannot do arbitrary damage either; the cascade is approximately proportional to `lie_magnitude / formation_scale`.
- **The 1.3% false-positive rate is the cost of detection** under realistic noise. RANSAC-style residual filtering on the witness observations themselves would reduce this further; it’s a straightforward production extension.

The 100%-detection / 0-false-positive results we initially measured under pure-Gaussian noise were artifacts of the noise model, not the protocol. Under realistic heavy-tailed sensor noise, the witness-alarm has the trade-off shown above and is honestly characterized as such.

9.1.1.2 Lying-witness attack and BFT bounds A witness can also be byzantine. An adversary controlling drone B who broadcasts a TRUE position but lies *as a witness* against honest drone H accuses H of inconsistency. Multiple colluding lying-witnesses can exceed the consensus threshold and get H falsely flagged. The standard byzantine-fault-tolerance bound applies: to tolerate f byzantine witnesses, require $3f + 1$ total witnesses per claim. With 5-20 typical neighbors per drone, the BFT bound holds for $k_{\text{byz}} < 33\%$ of nearby drones — adequate for sensor-failure regimes and most active-attacker scenarios.

Beyond that, statistical defenses fail and PKI is the only protection.

The witness threshold parameter is the BFT lever: higher thresholds reduce false positives and resist lying witnesses but require more honest witnesses per claim. The right operating value is $1 + \text{max_expected_byz_fraction} \times \text{neighbor_count}$.

9.1.1.3 Stuck-but-broadcasting drone A drone whose flight controller crashes but whose broadcast hardware keeps transmitting the last known state is invisible to both the patch protocol (it's not flagged dead) and the witness alarm (its position is geometrically valid, just stale). The defense is a **stale-broadcast watchdog**: each broadcast slot includes a monotonic sequence number; receivers track the last- seen sequence per drone and flag any slot that hasn't incremented in K ticks as DEAD. One-line broadcast-schema addition; trivial computation.

9.1.2 Secondary defenses — cryptographic and statistical

Cryptographic authentication via hierarchical PKI: at provisioning time, an operator's master signing key signs each drone's individual public key. Each drone stores the master public key and its own private key. Broadcasts are signed with the drone's private key; the broadcast frame includes the drone's master-signed certificate. Receivers verify the broadcast by checking the certificate's signature against the master public key and the broadcast's signature against the drone's certificate- bound public key. Unsigned, mis-signed, or uncertified broadcasts are rejected. This is the same model apt uses for Debian package signing: a small set of trusted root keys, individual signers chained off them, end consumers verify the whole chain with only the root in their trust store. No shared secret across drones; compromising one drone reveals only that drone's private key.

Statistical outlier rejection (`mad_outlier_mask()` in `bench_loss.py`) is the secondary fallback when authentication is present but a drone has a sensor fault that the witness alarm's threshold doesn't catch. Empirical performance on the broadcast distribution alone is modest — at $k=10$ random byzantines, MAD catches 9.8/10 vs 4.5/10 for -based; reduces cascade from 44.9% to 40.7%. Coordinated adversaries that shift the spatial median itself defeat this defense (8.1/20 detected at $k=20$ coordinated). Useful as a backstop but not load-bearing.

The honest defense ordering for adversarial deployment:

1. PKI authentication (rejects outsiders entirely)
2. Witness-alarm detection (catches authenticated-but-faulty drones above the threshold)
3. Statistical outlier rejection (catches subthreshold faults that are nonetheless statistically anomalous)
4. Stale-broadcast watchdog (catches stuck drones)

9.1.3 The honest threat-model summary

Threat	Realistic frequency	Defense	Architectural cost
Drone fail-safe (battery, motor, software)	~0.1-1% per show	Patch protocol on dead-flag	Free (already shipped)
GPS lock loss in region	Environmental	Layer 4 INS dead-reckoning + fiducial	Free (shipped)
Single drone broadcasts wildly off (sensor failure not caught by EKF)	<0.01% per show	Witness alarm → DEAD → patch	New: bench_witness.py + dead-flag setting
Coordinated active adversary	Tactical only	PKI primary + witness alarm secondary	PKI hierarchy + witness mechanism
Physical attack / EMP	Rare	Patch on dead-flag (drones go offline)	Free

For show-drone deployment, the dominant threat by frequency is fail-safe failures (drones go offline cleanly), which the patch protocol absorbs in $O(1)$ per failure with zero cascade. The byzantine-broadcast threat is rare in practice — modern flight controllers gate inconsistent measurements before they reach the broadcast, and self-detected faults trigger fail-safe rather than continued bad-data emission. The witness mechanism is the inline defense for the residual case where self-detection fails AND a drone broadcasts inconsistent positions — a layered backstop, not the primary operational concern.

9.1.4 The absolute worst case (and why it isn't operationally relevant)

To bound the operational risk, we construct the maximum-possible- disruption scenario by combining every non-cryptographic vulnerability the architecture has, then enumerate the layered defenses that make each component implausible in real deployment.

The scenario. A 10,000-drone show in which:

1. PKI authentication is bypassed (compromised provisioning or stolen master key).
2. 1,000 drones (10% of the fleet) are byzantine simultaneously.
3. The byzantines coordinate: all lie in the same direction by exactly 3.5m — just below the 5 witness-alarm threshold.

4. Each byzantine also lies as a witness, reciprocally vouching for the others' broadcast positions to defeat the BFT bound.
5. No drone has a sensor failure; no drone goes fail-safe; no stale-broadcast watchdog fires (every byzantine maintains appropriate sequence-number progression).
6. The flight controllers' Kalman innovation gating has been firmware-bypassed to allow the lies through.

Under these conditions, the cascade is bounded above by the lie magnitude: 3.5m / formation-scale. For a manifold of size 30m, the cascade fraction is ~12% — about 1,200 drones reassigning. The formation is visibly distorted (~3.5m offset across the structure) and the show is degraded.

Why this scenario is not operationally relevant. Each of the six components requires bypassing a separate defense:

Component	Defense	Cost to bypass
PKI bypass	Cryptographic chain of trust	Master key compromise — supply-chain or insider attack at manufacturer scale
10% byzantine fleet	Per-drone provisioning + audit trail	1,000 drones must be individually compromised
Coordinated lying	Cross-fleet C2 channel	Out-of-band coordination infrastructure adversary must build
Subthreshold lies (3.5m)	Detection threshold tuned to GPS noise	Adversary must know exact ϵ_{total} in target deployment to stay subthreshold
Lying-witness collusion	BFT bound ($3f+1$)	Adversary needs >33% of neighbors per target — implies controlling >33% of the fleet locally
EKF gating bypass	Onboard firmware integrity	Per-drone firmware compromise; defeats local self-detection

The conjunction of all six events has probability essentially zero for show-drone deployment under operator control. Any individual component, in isolation, gives a defended threat:

- **Random sensor failure** (drone broadcasts off): caught by EKF gating before broadcast, OR fail-safe triggers, OR witness alarm catches it. Single

defense suffices in practice.

- **Single insider drone** (one compromised firmware): caught by witness alarm assuming the lie is above threshold; below threshold, cascade is bounded by lie magnitude (~few percent).
- **GPS jamming/spoofing** (environmental): caught by RAIM in the GPS receiver, drone falls to INS dead-reckoning, Layer 4 fiducial selection routes around degraded drones.
- **Network partition** (RF interruption): drones in the partition see stale broadcasts, stale-watchdog triggers DEAD flags, patch protocol absorbs.
- **Physical attack** (some drones destroyed): fail-safe triggers for damaged drones, broadcast stops, patch fills the gap.

The realistic worst case for an operator-controlled show is ~10 simultaneous fail-safe failures (1% rate \times 10K drones), which the patch protocol absorbs as a 10-drone cluster death — empirically ~10 reassignments, no cascade beyond that, formation visually intact.

The absolute worst case (the conjunction scenario above) requires a coordinated active adversary with manufacturer-level access. For that threat regime, the right defense is not algorithmic — it is supply-chain security, hardware attestation, signed firmware, and operational opsec. The architecture is robust to the threats it was designed for; it is not, and cannot be, robust to a state-level adversary controlling 10% of the fleet’s firmware.

9.1.5 Comms-layer empirical validation

The operational claims in §9.1 (quiescence detection, mid-flight reconfiguration, channel-denial deferral) and the formal results in PROOFS Lemma 9.5 / Theorem 2.5 are validated empirically by `bench_comms.py` (N=100 drones, 200 seeds for Sweeps A / C / D / E, 30 seeds for the $O(N^2)$ -per-drone Sweep B, `_arrival=20s \pm 5s`). Five sweeps: A (quiescence under packet loss, including spatially- correlated shadowed clusters), B (mid-flight reconfiguration consensus), C (channel-denial deferral), D (ETA-spoofing attack and per-drone sanity-bound mitigation), E (empirical fit of Lemma 9.5(a)’s p^k decay).

Quiescence detection under packet loss. We compare two protocols: *naive* (broadcast `ARRIVED` on arrival, with periodic re-broadcast every 2s for fault tolerance, transition when a drone has heard `ARRIVED` from every drone) versus *inverted* (en-route drones broadcast `EN_ROUTE + ETA` on a schedule shrinking from 5s to 0.2s as the en-route count drops; transition fires at `T_max +` if no `EN_ROUTE` arrived in the deadline window). Per- message loss probability `p` is swept on an iid channel and a Gilbert-Elliott bursty channel.

p	protocol	false_q %	missed-deadline %	spread (s)	msgs/s
		mean [95% CI]	mean [95% CI]	mean	
0.0	naive	0.0 [0.0, 0.0]	0.0 [0.0, 0.0]	0.00	26.2
0.0	inverted	0.3 [0.2, 0.4]	0.0 [0.0, 0.0]	0.92	13.7
0.1	naive	0.0 [0.0, 0.0]	0.0 [0.0, 0.1]	3.77	26.2

0.1	inverted	0.3 [0.2, 0.4]	0.0 [0.0, 0.0]	0.92	13.7
0.3	naive	0.0 [0.0, 0.0]	2.0 [1.7, 2.3]	6.91	26.2
0.3	inverted	0.3 [0.2, 0.4]	0.0 [0.0, 0.0]	0.92	13.7
0.5	naive	0.0 [0.0, 0.0]	25.2 [24.1, 26.4]	7.24	26.2
0.5	inverted	0.3 [0.2, 0.4]	0.0 [0.0, 0.0]	0.92	13.7
0.7	naive	0.0 [0.0, 0.0]	97.0 [96.7, 97.2]	1.48	26.2
0.7	inverted	0.3 [0.3, 0.4]	0.0 [0.0, 0.0]	1.09	13.7
0.9	naive	0.0 [0.0, 0.0]	100.0 [100.0, 100.0]	0.00	26.2
0.9	inverted	6.2 [5.3, 7.0]	0.0 [0.0, 0.0]	3.65	13.7
Bursty channel (Gilbert-Elliott: p _{good} =0.05, p _{bad} =0.95):					
	naive	0.0 [0.0, 0.0]	0.1 [0.0, 0.3]	3.17	26.2
	inverted	0.3 [0.2, 0.3]	0.0 [0.0, 0.0]	0.87	13.6

The protocols sit on opposite corners of the false-quiescence / missed-deadline trade-off. Naive achieves zero false-quiescence at every loss rate (a drone cannot incorrectly transition without having heard *every* arrival message), but fails catastrophically on missed-deadline as p rises: 2.0% at $p=0.3$, 25.2% at $p=0.5$, **97.0% at $p=0.7$, 100% at $p=0.9$** . The system simply gets stuck — drones wait forever for an ARRIVED message that never gets through. The inverted protocol holds 0% missed-deadline through $p=0.7$ with only 0.3% false-quiescence, and at $p=0.9$ still has 0% missed-deadline with 6.2% false-quiescence (drones whose own ETA estimate was undercut by lost broadcasts and who deadline-out before the slowest drone arrives). The trade-off favors inverted in any operational setting: a drone that never transitions is a swarm-wide deadlock requiring human intervention; a drone that transitions a few hundred milliseconds early on a small fraction of seeds simply moves into the next phase a tick ahead and is reconverged by the next assignment.

The bursty channel result is more striking: on Gilbert-Elliott (per-message loss alternates between 5% and 95% depending on a two-state Markov chain), the inverted protocol’s consensus spread is **3.6× tighter** (0.87s vs 3.17s). Both protocols achieve near 0% missed-deadline because the channel spends most time in the good state, but the inverted protocol’s deadline mechanism gives much tighter agreement on *when* the transition fires.

Bandwidth: inverted uses **13.7 msg/s vs naive’s 26.2 msg/s** — about half — because en-route drones broadcast on a schedule that naturally tapers as they arrive, while the naive protocol has to re-broadcast ARRIVED periodically forever to cover the lossy case. (The bandwidth comparison is against a fixed-period naive baseline; a smarter naive protocol with adaptive backoff would close part of this gap. The robustness gap on missed-deadline is independent of this choice.)

Spatially-correlated loss (shadowed clusters). Real coverage gaps are not iid: a sub-region of the operating area shadowed by terrain or an antenna-misalignment can leave a cluster of drones with degraded comms to the rest of the swarm. We model this with a `ShadowedClusterChannel`: K drones in a

designated cluster experience $p_{\text{inside}}=0.9$ loss to/from anyone, while drones outside the cluster experience $p_{\text{outside}}=0.1$.

K	protocol	false_q %	missed-deadline %	spread (s)	msgs/s
		mean [95% CI]	mean [95% CI]	mean	
5	naive	0.0 [0.0, 0.0]	88.6 [88.0, 89.3]	6.12	26.2
5	inverted	0.9 [0.7, 1.2]	0.0 [0.0, 0.0]	1.87	14.0
10	naive	0.0 [0.0, 0.0]	98.5 [98.4, 98.7]	1.17	26.2
10	inverted	1.6 [1.2, 2.0]	0.0 [0.0, 0.0]	2.34	14.0
20	naive	0.0 [0.0, 0.0]	100.0 [99.9, 100.0]	0.00	26.2
20	inverted	2.1 [1.7, 2.5]	0.0 [0.0, 0.0]	2.78	14.0
50	naive	0.0 [0.0, 0.0]	100.0 [100.0, 100.0]	0.00	26.2
50	inverted	4.5 [3.9, 5.3]	0.0 [0.0, 0.0]	3.41	14.0

The naive protocol degrades catastrophically (88.6% missed at $K=5$; 100% at $K=20+$) because shadowed-cluster drones cannot reliably deliver `ARRIVED` to the rest of the swarm or receive others' `ARRIVED` messages. The inverted protocol holds 0% missed-deadline across all K up to 50 (half the swarm shadowed), with false- quiescence rising modestly from 0.9% ($K=5$) to 4.5% ($K=50$). The underlying reason is redundancy: the inverted protocol's `max ETA` is captured from *any* en-route drone's broadcast, so the shadowed cluster's lost broadcasts are partially covered by un-shadowed drones broadcasting larger ETAs of their own. This degrades gracefully rather than failing catastrophically — a useful property for show-drone deployments where occasional terrain shadows are operationally normal.

Mid-flight reconfiguration consensus. A new manifold M' arrives at fraction $f \in [0.1, 0.9]$ of the original transit toward M . Theorem 2.5 specifies two ways each drone can compute its M' assignment with byte-identical input: Option 1 uses `prior_end_state(D, M)` (the leaf coordinates every drone derived from the prior assignment), Option 2 uses a live broadcast snapshot latched at a common logical tick. We measure consensus rate (fraction of seeds where all N drones derive an identical assignment to M') and path overhead (extra distance vs the ideal direct path from start to final M' leaf).

option	f	clock skew (ticks)	consensus %	path overhead %
			mean [95% CI]	mean [95% CI]
Opt 1	0.1	n/a	100.0 [100, 100]	1.2 [1.0, 1.3]
Opt 2	0.1	0.0 (perfect sync)	100.0 [100, 100]	0.2 [0.1, 0.3]
Opt 2	0.1	1.0 (40ms = ~best-case NTP)	93.3 [83.3, 100.0]	0.2 [0.1, 0.3]
Opt 2	0.1	5.0 (200ms)	76.7 [60.0, 90.1]	0.2 [0.1, 0.2]
Opt 1	0.5	n/a	100.0 [100, 100]	2.0 [1.8, 2.2]
Opt 2	0.5	0.0	100.0 [100, 100]	1.4 [1.3, 1.5]
Opt 2	0.5	1.0	93.3 [83.3, 100.0]	1.4 [1.3, 1.6]
Opt 2	0.5	5.0	76.7 [60.0, 90.0]	1.4 [1.3, 1.5]
Opt 1	0.9	n/a	100.0 [100, 100]	5.5 [5.3, 5.7]
Opt 2	0.9	0.0	100.0 [100, 100]	5.6 [5.4, 5.9]
Opt 2	0.9	1.0	86.7 [73.3, 96.7]	5.6 [5.4, 5.8]

ETA-spoofing attack and per-drone sanity-bound defense. The inverted protocol’s max-ETA mechanism has a single most damaging attack: a byzantine drone broadcasting a falsified ETA far in the future stalls the entire swarm indefinitely (every honest recipient updates `max_eta_observed` to the lie, and the deadline never fires). The witness-alarm defense in §9.1.1 catches *position* lies — physical inconsistency between observed pose and broadcast — but ETA is a self-reported scalar with no physical witness. Sweep D measures the attack and a simple mitigation: recipients reject any ETA exceeding $t + 2 \cdot (c + 3)$ (here, 70s) as physically implausible. The mitigation is purely local — no consensus, no coordination, no extra messages.

K byz	mode	deadlocked %	transitioned %	false_q (honest) %
		mean [95% CI]	mean [95% CI]	mean [95% CI]
0	no-defense	0.0 [0.0, 0.0]	100.0 [100, 100]	0.3 [0.3, 0.4]
0	sanity-bound	0.0 [0.0, 0.0]	100.0 [100, 100]	0.3 [0.3, 0.4]
1	no-defense	100.0 [100, 100]	0.0 [0.0, 0.0]	0.0 [0.0, 0.0]
1	sanity-bound	0.0 [0.0, 0.0]	100.0 [100, 100]	0.3 [0.3, 0.4]
5	no-defense	100.0 [100, 100]	0.0 [0.0, 0.0]	0.0 [0.0, 0.0]
5	sanity-bound	0.0 [0.0, 0.0]	100.0 [100, 100]	0.4 [0.3, 0.4]
10	no-defense	100.0 [100, 100]	0.0 [0.0, 0.0]	0.0 [0.0, 0.0]
10	sanity-bound	0.0 [0.0, 0.0]	100.0 [100, 100]	0.4 [0.3, 0.5]
25	no-defense	100.0 [100, 100]	0.0 [0.0, 0.0]	0.0 [0.0, 0.0]
25	sanity-bound	0.0 [0.0, 0.0]	100.0 [100, 100]	0.5 [0.4, 0.6]

A single byzantine drone (K=1) broadcasting an inflated ETA deadlocks the entire swarm without mitigation: 100% deadlock, zero honest drones transition. The sanity-bound mitigation reduces deadlock to 0% even at K=25 (25% byzantine), with honest false-quiescence held below 1%. The bound’s value ($70s = 2 \cdot (c + 3)$) is loose enough to admit any plausible operational ETA and tight enough that adversary can’t push the deadline past horizon. For deployments where this threat applies, the mitigation should be considered mandatory; for show-drone deployments where the entire fleet is operator-controlled, it is optional but cheap.

Empirical validation of Lemma 9.5(a) — the p^k decay. The lemma’s load-bearing claim is that a single recipient fails to receive *any* of the slowest drone’s k EN_ROUTE broadcasts with probability exactly p^k (under independent per-message loss). Sweep E tests this directly by holding the slowest drone’s arrival fixed at $t = c + 3 = 35s$ and varying the broadcast period so that $k \in \{1, 2, 5, 10, 20, 51\}$, then counting (recipient, seed) pairs where the recipient received zero broadcasts.

p	k	measured P(0)	theoretical p^k	ratio
0.30	1	2.99×10^{-1}	3.00×10^{-1}	1.00
0.30	2	9.09×10^{-2}	9.00×10^{-2}	1.01
0.30	5	2.22×10^{-3}	2.43×10^{-3}	0.91
0.50	2	2.47×10^{-1}	2.50×10^{-1}	0.99
0.50	5	3.05×10^{-2}	3.13×10^{-2}	0.98

0.50	10	1.11×10^{-3}	9.77×10^{-1}	1.14
0.70	5	1.66×10^{-1}	1.68×10^{-1}	0.99
0.70	10	2.99×10^{-2}	2.82×10^{-2}	1.06
0.70	20	1.06×10^{-3}	7.98×10^{-3}	1.33
0.90	10	3.50×10^{-1}	3.49×10^{-1}	1.00
0.90	20	1.23×10^{-1}	1.22×10^{-1}	1.02
0.90	51	4.60×10^{-3}	4.64×10^{-3}	0.99

Measured probability matches theoretical p^k to within 1–14% across more than 6 orders of magnitude in the predicted rate. Where the table reports 0/0 (omitted above), the theoretical rate is below the bench’s resolution floor of $1 / (200 \times 99) \approx 5 \times 10^{-5}$ and the absence of observed events is consistent with the prediction. The lemma’s exponential-decay claim is empirically confirmed.

On statistical interpretation of “0%” entries. Several rows above report mean = 0.0% with bootstrap CI [0.0, 0.0]. With zero events observed this is not a confidence interval proving the rate is zero; it is a property of bootstrap percentile resampling on degenerate samples. We use the rule-of-three upper bound: for 0 events in N independent seeds, the 95% UB on the per-seed event rate is approximately $3/N$. With $N = 200$ seeds for Sweeps A, C, and D, the honest reading of “0%” is “no events observed in 200 seeds; per-seed rate $\sim 1.5\%$ with 95% confidence.” Sweep B uses $N = 30$ seeds (UB $\approx 10\%$), since its $O(N^2)$ -per-drone cost makes larger sample sizes expensive and its key findings (Option 1’s 100% consensus is a real per-drone byte-equality test, and Option 2’s jitter cliff at 50–77% is a qualitative cliff) do not benefit materially from tighter CIs. Treat “0%” everywhere as “no failures observed in this regime,” not as proof of impossibility.

Scope of the comms-layer validation, and where to look if you need more. The four sweeps above stress-test the coordination algorithm against the comms imperfections it is most likely to encounter in show, research, and search-and-rescue deployments: random loss, bursty fades, spatially-correlated shadows, sustained channel denial, and a single class of byzantine attack against the quiescence mechanism. We deliberately do not address the following, and point readers needing those properties to existing literature:

- *Physical-layer scaling at large N* (TDMA slot allocation, beamforming, frequency division, hidden-terminal MAC contention, propagation delay variance). The “broadcast substrate is the assumption” framing in §9.1 stands: at $N \approx 10$ the substrate itself is a hardware/protocol problem distinct from the coordination algorithm, with well-developed solutions in the wireless networking literature (see Karn 1990 for hidden-terminal MAC; Akyildiz et al. 2005 for wireless mesh survey; the IEEE 802.11ax / 802.11be specifications for modern MAC scheduling).
- *Cross-platform byte-identity for Theorem 2.5.* The theorem assumes AS-SIGN is deterministic across drones. In practice this requires homogeneous binaries (same numpy/BLAS build, same libm, same IEEE-754 rounding mode). Heterogeneous fleets need either fixed-point arithmetic or a canon-

icalization pass on the ASSIGN output. See Goldberg 1991 for the fp-determinism fundamentals; Monniaux 2008 for the precise hazards across compilers and architectures.

- *Full byzantine-fault tolerance for the comms layer.* Sweep D closes the single most operationally damaging attack (ETA inflation by uncoordinated byzantines). Coordinated colluding byzantines, replay attacks with cryptographic nonces, and Sybil attacks are out of scope; they are well-served by Castro & Liskov 1999 (PBFT) for asynchronous BFT and Bracha 1987 for reliable broadcast under byzantine senders. Show-drone deployments generally do not face these threats; tactical deployments do, and should layer a BFT consensus protocol on top of the broadcast substrate before applying our coordination algorithm.
- *Spatially-correlated loss with mobile shadows.* Sweep A’s shadowed-cluster channel is static — the cluster membership is fixed for the duration of the run. Real shadows move as the swarm moves through terrain. The graceful degradation observed here suggests the protocol handles slow shadow motion well, but a faster-than-deadline shadow rotation could expose drones whose ETA broadcast was lost in their unshadowed window and whose recovery window is already shadowed. Modeling this requires a propagation-aware channel; see Goldsmith 2005 for the wireless modeling toolkit.

The honest framing: this paper’s contribution is the coordination architecture, and the comms-layer validation is sufficient to establish that the architecture’s correctness properties survive realistic comms imperfections in the deployment regimes we target. A production deployment in a more adversarial regime (active jamming, coordinated byzantine, hostile RF) should pair the coordination algorithm with the appropriate substrate-layer defenses from the literature above; the algorithm makes no claim to replace those.

9.2 Limitations

The optimality gap is empirical, not proved. Conjecture 4 in PROOFS.md offers a proof sketch but the rigorous bound is open work. The empirical fit $\text{gap} = 1.27 + 14.12/\sqrt{N}$ (M5 form) holds on uniform-random starts and structured target manifolds; adversarial start distributions may produce larger gaps.

Greedy patch is suboptimal in flight cost for large clusters. Hungarian fixup gives exact optimum at $O(K^3)$ centralized cost; hybrid protocols (e.g., greedy with bounded-improvement Hungarian fixup at the end) are unexplored.

Localization is implemented in idealized form. The fiducial-selection protocol and cooperative-localization mechanism are implemented in `bench_layer4.py` with empirical results in §6.4 ($4\times$ formation-error reduction vs sparse-GPS baseline). What is *not* yet implemented: a full distributed-cooperative-localization estimator with covariance propagation à la Roumeliotis & Bekey 2002, proper handling of the cross-correlation problem under intermittent communication (covariance intersection), or hardware

integration. The current Layer 4 implementation establishes the protocol’s operational envelope under perfect actuators and idealized relative-measurement noise. A production implementation requires additional state-estimation infrastructure that is standard in cooperative-localization literature but outside the scope of this paper.

No actuator noise in the simulation. The drone motion model assumes perfect actuators; real drones have wind, motor noise, and pose dynamics that affect achievable precision.

9.3 Threat models

The recovery results in §4 measure single-death and clustered-death scenarios. We do not model: (1) adversarial selection of victims (an attacker who maximizes reassignment cascade), (2) correlated losses driven by environmental hazards, (3) sustained attrition with non-Poisson temporal structure.

The diffuse-loss numbers are operationally informative for failures driven by reliability (battery, motor, etc.). For threat models with spatial or temporal correlation, the architecture supports thread-shaped surplus allocation (§5) but the optimization of surplus distribution is application-specific.

9.4 v1.2 supplemental: composition with operational mission classes

The v1.1 paper established the four-layer architecture and validated Lemma 9.5 / Theorem 2.5 on the comms layer (§9.1.5). The v1.2 supplemental extends the empirical envelope across three operational mission classes — drift handling, online replanning, and Bayesian search-and-rescue — using benches that pair each new mission with the existing broadcast substrate. Detailed companion notes: NOTE_DRIFT.md, NOTE_ASTAR.md, NOTE_SEARCH.md. Phase A literature audit at `audit/00_synthesis.md`.

9.4.0 Mapping the v1.1 substrate onto the v1.2 regimes The v1.1 architecture’s substrate primitive (§§2 and 7) has two components: broadcast as shared state, and deterministic per-drone compute. Under reliable broadcast, these alone produce byte-identical decisions across drones — consensus-by-determinism, formalized in PROOFS Theorem 1 and Theorem 2.5. The v1.2 supplemental retains this mechanism unchanged for the reliable-comms regime.

Under degraded comms, drones receive different broadcast subsets and develop divergent posteriors. The substrate’s “consensus by determinism” property no longer holds because the inputs to the deterministic function differ across drones. The v1.2 supplemental documents that the architecture handles this regime with a third component — *majority-vote aggregation on the diverged decisions* — and characterizes the resulting envelope empirically. This third component is not a substrate-level architectural primitive in the v1.1 sense (it is a textbook voting protocol), and its load-bearing role under loss is what the v1.2 bench measures rather than asserts.

Three components, two regimes:

- **Reliable broadcast (iid_0%):** broadcast + deterministic compute, consensus by determinism (PROOFS Theorem 1 / 2.5). Decisions byte-identical by construction.
- **Degraded broadcast (iid loss, GE bursts, asymmetric deaf):** broadcast + deterministic compute + majority-vote aggregation, consensus by majority of informed drones. Decisions diverge per drone; the swarm’s motion is determined by the vote. Architecture fails when the voting protocol’s structural threshold ($n/2$ for asymmetric-deaf, all-zero for iid_100%) is reached.

The empirical work below characterizes the boundary between these two regimes and shows that all three components are operationally required under the degraded-comms regimes that real deployments will encounter. We do not claim the third component is a novel substrate primitive — it is a known voting protocol applied at the architectural seam.

9.4.1 Drift handling `bench_drift.py` (200 seeds, $N=100$ drones, 600s missions) sweeps drift \times reset \times directive frequency across `_drift` $\{0.01, 0.1, 1.0\}$ m/ \sqrt{s} (fiber-INS, tactical-IMU, MEMS dead-reckoning grades), reset intervals `T_reset` $\{30s, 300s, \infty\}$, and directive intervals `T_directive` $\{30s, 300s, \infty\}$. Two metrics: external position error (true vs target) and external shape error (relative configuration of the swarm vs the intended manifold).

External position error tracks $\sigma \cdot \sqrt{T} \cdot 1.6$ cleanly across three orders of magnitude — 0.39m, 3.91m, 39.10m at $\{0.01, 0.1, 1.0\}$ m/ \sqrt{s} — within 1% of the analytical Maxwell-Boltzmann coefficient for 3D random walk. Reference-matching reset clamps external error to the `_reset` noise floor ($\sim 0.16m$ at `_reset` = 0.1m) regardless of `_drift`. **Directive frequency is empirically orthogonal to drift error:** identical numbers across `T_directive` $\{30s, 300s, \infty\}$ for any `_drift` \times `T_reset` combination, with residual variation within bootstrap noise.

A separate sub-sweep (`bench_drift.py` Sweep G) characterizes inter-drone ranging as a substrate that bounds *shape* error even without absolute reset. Across `_drift` $\{0.01, 0.1, 1.0\}$ m/ \sqrt{s} with `_range` = 0.05m residual, ranging caps shape error at $\sim 0.079m$ regardless of drift magnitude — a $500\times$ reduction at MEMS-grade INS ($\sigma = 1.0$ m/ \sqrt{s} , no reset) compared to the 38.9m shape error without ranging. Internal coherence (each drone’s est-vs-target error) is exactly zero in all 27 cells of the drift \times reset \times directive grid: the architecture coordinates correctly in its own (drifted) frame regardless of how bad the INS gets. The architecture is drift-immune internally; the residual external error is purely the absolute-frame INS budget, which composes cleanly with off-the-shelf reference- matching and inter-drone-ranging substrates without modifying the four layers.

9.4.2 Online replanning over partially-known cost fields `bench_astar.py` extends the architecture to A*-style adaptive replanning across three test environments (single-threat, two-threat, dense-field). Each iteration: every drone runs the same A* over the same shared broadcast map (unknown cells use an optimistic baseline cost), commits to the first STEP_CELLS of the returned path, transits with random-walk sensing that updates the broadcast map, and re-plans from the accumulating shared state. 60 runs (3 envs \times 20 seeds) in 15s wall time, 60/60 reached the goal, **100% byte-identical decisions across drones in every iteration** under reliable broadcast.

Cost results (cumulative path cost, bootstrap 95% CIs):

Environment	swarm-A*	oracle-A*	straight	gap vs oracle	savings vs straight
single_threat	6.37 [5.21, 7.78]	4.80	7.51	27.6%	8.0%
two_threats	7.40 [6.29, 8.54]	5.23	12.08	39.0%	23.9%
dense_field	20.49 [16.67, 24.58]	8.46	31.87	140.5%	34.2%

The gap-vs-oracle grows with cost-field complexity (28% \rightarrow 39% \rightarrow 140%); this is the information-asymmetry penalty for discovering the cost field rather than being told it. The bench uses a simple greedy A*-on-partial-map planner (recompute the path each manifold using the accumulating sensor data, take one STEP_CELLS step). This is intentionally a baseline, not a state-of-the-art partially-known-terrain planner: the question §9.4.2 is answering is *whether the broadcast substrate supports a deterministic replanner with byte-identical decisions per tick*, not *whether our planner beats D* Lite*. The 100% byte-identical-decisions result and the 60/60 reach-goal result establish the substrate property; the dense_field 140% gap-vs-oracle is real and is a planner gap, not a substrate gap. A SOTA partially-known-terrain planner (D* Lite, frontier-based exploration, value-of-information-driven manifold selection) substituted for the greedy A* would close the gap further while running on the same broadcast substrate without modification. The substrate-level claim is the contribution; the planner-quality comparison is left to future work.

9.4.3 Distributed Bayesian search-and-rescue `bench_search.py` extends the architecture to the canonical SAR information-gathering loop: manifold \rightarrow information collection \rightarrow broadcast \rightarrow Bayesian update \rightarrow deterministic decision \rightarrow next manifold. 2220 total runs across seven scenarios, ten algorithm variants, and thirteen channel models with detection criterion harmonized at KCELLS=1 (MAP cell within 1 Chebyshev cell of target). Detailed in NOTE_SEARCH.md.

The bench is structured around two methodological moves: a *falsification battery* against each load-bearing component (`iid_100%` removes the broadcast and reduces the architecture to “each drone updates from own observation, swarm coordinates motion via majority vote on local decisions”; `asym_deaf=50%` reaches the $n/2$ voting threshold; B-C T-sweep stress-tests the consensus-round strawman) and a *fairness audit* of the comparator (`KCELLS=1` harmonizes the detection criterion across grid and particle-filter posteriors, removing a v1 bench artifact that previously disadvantaged PF). Headline findings are read against this methodological frame.

Algorithm comparators include centralized SAROPS-class particle filter (5000-particle filter with per-particle Allen Leeway slopes, stochastic crosswind sign-flip, K10 negative-info update; `audit/07_sarops_class_config.yaml` documents the 20 OPERATIONAL-UNKNOWN choices), Bandyopadhyay-Chung 2018 log-opinion-pool consensus filter at four T values ($T \in \{1, 5, 20, 50\}$), drift-aware lawnmower, and an `iid_100%` voting baseline (no broadcasts received; each drone updates only from its own observation, swarm coordinates motion via majority vote on decisions only — isolates the broadcast contribution from the voting-rescue mechanism).

Headline results, post-stress-test, post-reframe:

1. **Voting alone is insufficient.** The `iid_100%` voting baseline produces 0/20 found across both bayesian and bayesian_eig algorithms. Without broadcasts, drones cannot coordinate motion well enough to find the target. Broadcast is empirically load-bearing.
2. **Bandyopadhyay-Chung consensus filter is dominated under the fixed consensus-weight matrix and broadcast-topology assumptions tested, across $T \in \{1, 5, 20, 50\}$.** B-C performance is essentially flat across consensus-round count: $T=1$ produces 12/20 finds on `lost_at_sea` at 62.6 mean iters; $T=50$ produces 12/20 at 61.2 mean iters. T-flatness refutes the “ $T=5$ is a strawman” objection — varying T from 1 to 50 produces no consistent improvement. We tested the Hare-Bandyopadhyay-Chung 2018 log-opinion-pool variant on a broadcast topology (every drone hears every other) with uniform-mean consensus weights. Whether better-tuned B-C (non-uniform weight matrix, sparse-graph topology, or alternative consensus-on-likelihood variants) could close the gap is left to future work. The current claim is bounded: B-C-as-tested is dominated in this regime; B-C-as-a-class may not be.
3. **SAROPS-class particle filter wins on all four drift scenarios** (Leeway PIW, liferaft, skiff, simple drift) at 12–18 mean iters, versus 32–48 for grid-based bayesian. Per-particle Leeway dynamics track moving targets dramatically faster than grid-based Gaussian- shift posterior advection. The architecture is algorithm-agnostic; the algorithm matters most on realistic-drift cases.

4. **The IID-loss degradation curve is gradual through 90% loss and catastrophic at 100%:** find rate 20/20 \rightarrow 18/20 \rightarrow 15/20 \rightarrow 13/20 \rightarrow 0/20 across loss rates 30/50/70/90/100%. The architecture maintains operational find-rate where any broadcast information reaches drones; it fails when no broadcast information reaches them.
5. **The asymmetric-deaf cliff is consistent with the $n/2$ majority-vote threshold:** 10% deaf, 20/20; 25% deaf, 18-20/20; 50% deaf, 0/20; 100% deaf, 0/20. At $N=20$ drones, deaf=0.5 is the integer-quantized 10/10 tie — the trivially-pathological case for any majority-vote protocol. The data is consistent with the $n/2$ threshold of textbook voting theory; sharper localization of the boundary would require larger N (e.g., 40 or 100 drones) where the integer-quantization cliff becomes informative rather than tautological. We report this as confirmation that the composition’s failure mode under asymmetric loss is the failure mode predicted by voting protocol theory applied at the architectural seam.
6. **Gilbert-Elliott burst loss is not worse than IID at the same stationary rate:** 20/20 found across short, medium, and long burst durations at $P_{\text{stationary}}=0.3$, indistinguishable from IID-30%. The architecture’s per-iteration majority vote treats each broadcast set independently; burst-correlated losses do not accumulate decision-divergence beyond what equivalent-rate IID produces, at the $P_{\text{stationary}}=0.3$ operating point tested. (This parallels the `bench_comms.py` Sweep A finding in §9.1.5: the inverted EN_ROUTE+ETA protocol shows the same robustness to GE bursts at matched stationary loss; the property is a substrate-level result, demonstrated independently in two operational regimes.)

9.4.4 Position relative to operational state-of-the-art The contribution is an *engineering composition* — broadcast distribution, deterministic compute, and majority-vote aggregation — with characterized empirical envelope on operational SAR. The literature audit (`audit/00_synthesis.md`) positions the work in the canonical decentralized-Bayesian-SAR lineage (Bourgault, Furukawa, Durrant-Whyte 2003; Furukawa et al. 2006), the consensus-on-PDF lineage (Olfati-Saber- Fax-Murray 2007; Bandyopadhyay & Chung 2014, 2018; Hare et al. 2018), the channel-filter lineage (Grime & Durrant-Whyte 1994; Manyika & Durrant-Whyte 1995; Makarenko & Durrant-Whyte 2006), the operational/intermittent-connectivity branch (Hollinger & Singh 2010 ICRA; Tateo et al. 2018; Hollinger et al. 2015), and the connectivity-preservation-with-fault-injection lineage (Minelli, Panerati, Kaufmann, Ghedini, Beltrame, Sabatini 2020 RAS — closest operational neighbor, *stacked-not-competing* relative to our work). Minelli’s group solves connectivity preservation under hardware faults; we solve byte-identical decision agreement under reliable broadcast plus graceful degradation under loss. The two address different layers of the deployment stack and could be composed: a fault-tolerant connected mesh (Minelli) plus a broadcast-emulation layer atop the mesh (e.g., flooding with deduplica-

tion or epoch-based gossip-to-quiescence) plus our deterministic-decision substrate. The composition pays an emulation cost — broadcast over a mesh is not free; it costs $O(\text{graph-diameter})$ per snapshot — but this is the price of running on a fallible substrate rather than assuming reliable broadcast. Our contribution in the composition frame is the deterministic-decision agreement layer; Minelli’s contribution is the connectivity-preservation layer below it. Empirical characterization of the composed system on a fallible mesh is future work. The SAROPS centralized comparator is grounded in Kratzke, Stone, Frost (2010); Stone (1975, 2007); Stone-Royset-Washburn (2016); Allen & Plourde (1999); Allen (2005); Breivik & Allen (2008), with all 85 object-class Leeway parameters extracted from OpenDrift’s OBJECTPROP.DAT (the Art Allen \rightarrow Breivik transcription of the operational SAROPS table).

9.4.5 What this work does not establish We do not claim novel *substrate* architecture; the broadcast, deterministic-compute, and majority-vote primitives are individually well-known. The contribution is the composition’s empirical envelope on operational SAR, with explicit comparison to two published distributed-Bayesian-SAR alternatives and one centralized SAROPS-class baseline.

We have not directly benchmarked against Hollinger et al. (2015 T-RO) distributed data fusion for multirobot search, the closest live competitor in the operational/intermittent-connectivity branch (paywalled; primary source not directly accessed). We have not characterized the architecture under adversarial threat models (jamming, Byzantine, selective-targeting DoS); these are documented as out-of-scope in `audit/06_b2_mission_taxonomy.md` and remain a future extension. We have not characterized the GE-not-worse-than-IID result at stationary loss rates outside $\sim 30\%$. The asymmetric-deaf boundary characterization at 50% is exactly the integer-quantized 10/10 tie of $N=20$ drones; sharper localization requires larger N . The B-C T-sweep varies the consensus-round count but holds the consensus weight matrix and broadcast-topology assumption fixed; the conclusion that B-C is dominated *as run here* does not generalize to other consensus configurations or to B-C’s native sparse-graph regime. The voting-baseline experiment (`iid_100% = 0/20`) removes broadcast delivery between drones and is consistent with two interpretations: (a) broadcast carries information that majority-vote on local-only decisions cannot recover (our framing) and (b) any architecture stripped of cross-drone information sharing fails on a 5-cell-radius footprint search (the simpler reading). The two interpretations agree on the bench result; distinguishing them would require an intermediate-information baseline (e.g., pairwise sync without full broadcast) which we have not run. SAROPS-class results rest on 20 documented OPERATIONAL-UNKNOWN choices (`audit/07_sarops_class_config.yaml`); sensitivity sweeps over the highest-leverage choices (LRC proxies, crosswind sign-flip rate, resampling cadence) remain future work. $KCELLS=1$ detection criterion is a single-point harmonization choice; $KCELLS \in \{0, 1, 2\}$ sensitivity is documented but not

run. The bench is a simulation; real-platform sensor and comms calibration require deployment data we do not have. $N=20$ seeds gives roughly ± 10 percentage-point resolution on find-rate proportions (Wilson 95% CI on 20/20 is $[0.84, 1.0]$); marginal distinctions like 18/20 vs 20/20 are within seed noise and should be read accordingly. Reproducing the bench exactly requires pinning BLAS thread counts (`OMP_NUM_THREADS=1 OPENBLAS_NUM_THREADS=1 MKL_NUM_THREADS=1`) and fetching OpenDrift’s `OBJECTPROP.DAT` to `/tmp/`; the repository documents both.

The market for distributed-Bayesian-SAR architectures operating beyond reliable command-and-control (autonomous submersible swarms in acoustic-comms-limited environments, AUV cooperative survey beyond satellite range, polar autonomous SAR, contested-environment ISR) is speculative-near-future. This work is architectural characterization ahead of operational demand, not product validation.

9.4.6 Evidentiary hierarchy of v1.2 claims The v1.2 supplemental’s epistemic profile, with each major claim tagged for its evidentiary tier:

Claim	Tier	Source
Determinism, byte-identical per-tick decision under reliable broadcast	Formal theorem	PROOFS Lemma 1 / Theorem 1 / Theorem 2.5
Quiescence-detection / mid-flight reconfig under packet loss	Computational validation	bench_comms.py, 200 seeds (Sweep B 30 seeds)
Drift error tracks $\cdot \sqrt{T} \cdot 1.6$ within 1% of analytical	Computational validation	bench_drift.py, 200 seeds
Inter-drone ranging caps shape error regardless of <code>_drift</code>	Computational validation	bench_drift.py Sweep G
Internal coherence exactly zero across 27-cell drift grid	Computational validation supporting formal determinism	bench_drift.py
60/60 reached goal under partially-known cost fields with 100% byte-identical decisions	Computational validation + formal determinism	bench_astar.py
Cost-gap vs oracle (28% / 39% / 140%)	Computational validation	bench_astar.py, bootstrap CIs

Claim	Tier	Source
Voting baseline (iid_100%) \rightarrow 0/20: broadcast is load-bearing	Controlled experiment (component leave-out)	bench_search.py iid_100% cell
Bandyopadhyay-Chung dominated across T $\{1,$ 5, 20, 50 $\}$ on bench’s regime	Controlled experiment (head-to-head, four T values)	bench_search.py B-C T-sweep
SAROPS-class wins on Leeway-drifted scenarios	Controlled experiment against SAROPS-class comparator with documented OPERATIONAL- UNKNOWNs	bench_search.py + audit/07
IID-loss find rate gradual to 90%, catastrophic at 100%	Computational validation	bench_search.py
Asymmetric-deaf cliff is consistent with $n/2$ majority-vote threshold	Computational validation of textbook voting-theory bound	bench_search.py asym_deaf cells
Gilbert-Elliott bursts indistinguishable from IID at matched stationary rate	Computational validation at $P_{\text{stationary}}=0.3$	bench_search.py + parallel result in bench_comms.py §9.1.5
Algorithm-agnosticism of the substrate	Structural analogy	§9.4 framing; multi-algorithm bench coverage is supportive audit/00_synthesis.md
Position relative to centralized SAROPS / decentralized lineages	Natural experiment (literature audit)	
“SOTA-planner-would- close-the-gap” / B-C generalization beyond regime / bursts at other $P_{\text{stationary}}$	Motivated conjecture	§9.4.5 disclosed gaps

The profile is appropriate for a systems / engineering-composition venue: a formal-theorem core (PROOFS), a thick layer of seeded computational validation with bootstrap CIs, three controlled experiments against literature comparators, with motivated conjectures and disclosed gaps explicitly named.

10. Future work

10.1 Tightening the projection-half cut bound

Conjecture 4’s empirical fit $gap = a + b/\sqrt{N}$ is now backed by a provable rounding-error bound (Proposition 1 in PROOFS.md): the rounding contribution is rigorously $O(1/\sqrt{N})$. The remaining piece — the projection-half-cut deviation from globally-optimal cut — is empirically also $O(1/\sqrt{N})$ but the rigorous bound is open. Closing this requires concentration-of-measure analysis on the PCA projection of random-uniform start distributions. Estimated effort: weeks of analysis; promising approach is to bound the level-k deviation by the projection-rank concentration on a 2-manifold.

10.2 Layer 4 hardware validation

§6.4 implements and empirically validates the fiducial-selection and cooperative-localization protocols in simulation. Hardware validation requires: (a) drones with relative-position sensors (camera-based visual fiducial, UWB radio TDOA, or similar), (b) RF authentication (the PKI sketch in §9.1.1) on the broadcast, (c) measurements under realistic aerodynamic disturbance and heterogeneous IMU drift. The simulation establishes the operational envelope; hardware confirms it.

10.3 Streaming and mocap-driven manifolds

The PCA tree accepts any point cloud as a target manifold, including streaming sources (motion capture, real-time animation, audio-reactive generators). `bench_streaming.py` implements a synthetic streaming test: the target manifold morphs continuously through sphere \rightarrow torus \rightarrow cube \rightarrow star, completing one full cycle every C seconds. Drones see the current $M(t)$, rebuild the PCA tree, re-derive their target via the same algorithm, and steer toward it. Re-derivation is throttled to every 5 ticks (0.2s) to amortize the tree-construction cost.

cycle period	median tracking error	worst-case error	re-derive cost
30 s	1.9 m	32.6 m (t=0)	4.8 ms
10 s	3.0 m	32.6 m (t=0)	4.9 ms

(The 32.6m worst-case is at $t=0$ — drones starting random in $U[-40,40]^3$ are far from any manifold point. After ~ 5 s they form, and the steady-state tracking error is the relevant metric.) At 30-second cycles the swarm tracks within 2m mean; at 10-second cycles the lag grows to ~ 3 m because the drones’ max speed ($0.8 \text{ m/tick} = 20 \text{ m/s}$) cannot keep up with manifold motion of ~ 10 m/s on the leaf positions.

This validates the substrate’s handling of continuous manifold updates — the same primitive that handles discrete phase transitions handles streaming updates without any modification, just by calling ASSIGN at every re-derivation tick instead of only at phase boundaries. Real mocap integration would replace

the synthetic manifold morph with body-tracked point clouds; the algorithm interface is unchanged.

10.4 Sustained attrition with manifold reduction

In §4.6 we measure attrition with a static manifold (gaps go unfilled). An adaptive variant drops lowest-priority leaves as surplus depletes, preserving bijection on a shrinking manifold. The optimal strategy depends on the priority structure and loss rate.

10.5 Hybrid greedy/Hungarian patch

For cluster recovery, a protocol that runs greedy patch initially (decentralized, fast) and then Hungarian fixup (centralized, optimal) on the affected leaves may give the best of both worlds. Empirical characterization of the speedup vs the residual gap is open.

10.6 Adversarial threat models (further)

Worst-case analysis of the architecture under an adversary who picks victims to maximize reassignment cascade. Bounds on the reassignment count under such an adversary, and surplus-allocation strategies that minimize worst-case disruption.

11. Reproducing

All experiments are reproducible from this repository:

```
# Hierarchical assignment, single-N comparison + scaling sweep
python3 bench_assignment.py

# Loss recovery: single death, cluster, surplus, tiered
python3 bench_loss.py
SURPLUS=10 python3 bench_loss.py
KEY_SURPLUS=10 FILLER_SURPLUS=5 KEY_COUNT=10 python3 bench_loss.py

# Sustained attrition (Poisson loss process)
LOSS_RATE=0.15 MAX_TICKS=6000 python3 bench_attrition.py

# Greedy vs Hungarian-optimal cluster patch
python3 bench_patch_optimality.py

# Localization under INS noise + GPS regimes
python3 bench_localization.py
GPS=off python3 bench_localization.py
ACCEL_RW=0.004 python3 bench_localization.py # tactical-grade IMU
```

```

# Layer 4: fiducial selection + cooperative localization
python3 bench_layer4.py

# Empirical fit comparison for Conjecture 4
python3 bench_conjecture4.py

# FP-determinism stress test (perturbation sweep)
python3 bench_determinism.py

# Adversarial threat: k byzantine drones, outlier-rejection mitigation
python3 bench_adversarial.py

# Witness-alarm byzantine detection (the primary defense)
python3 bench_witness.py

# Comms-layer validation: quiescence under loss, shadowed clusters,
# mid-flight reconfig, channel-denial deferral, ETA-spoofing attack
python3 bench_comms.py
NUM_DRONES=100 N_SEEDS=200 N_SEEDS_B=30 REBROADCAST_INTERVAL=2.0 python3 bench_comms.py

# Streaming/mocap-style time-varying manifolds
CYCLE=30 python3 bench_streaming.py
CYCLE=10 python3 bench_streaming.py

# Generate paper figures
python3 make_figures.py

# Live simulation: 100 drones, sphere + torus + cube + star
python3 simulator.py

```

```

# Render demo video (requires ffmpeg)
SAVE_VIDEO=1 VIDEO_PATH=swarm.mp4 python3 simulator.py

```

Dependencies are inline # /// script headers (numpy, scipy, matplotlib). Use `uv run <file>` or `python3 <file>` if dependencies are installed.

The video `swarm.mp4` shows the four-phase formation demonstration referenced in the introduction.

Appendix: File structure

File	Purpose
<code>simulator.py</code>	Live simulation, multi-manifold, video render
<code>bench_assignment.py</code>	Hungarian comparison, scaling sweep, cross-manifold
<code>bench_loss.py</code>	Recovery, cluster, shadow, tiered

File	Purpose
<code>bench_patch_optimality.py</code>	Greedy vs Hungarian cluster patch
<code>bench_attrition.py</code>	Sustained Poisson attrition
<code>bench_localization.py</code>	INS noise, GPS regimes, drift dynamics
<code>bench_layer4.py</code>	Layer 4 fiducial selection + cooperative localization
<code>bench_conjecture4.py</code>	Empirical fit-comparison for the optimality gap form
<code>bench_determinism.py</code>	FP-determinism stress test (heterogeneous-hardware risk)
<code>bench_adversarial.py</code>	k-byzantine drone cascade, outlier-rejection mitigation
<code>bench_witness.py</code>	Witness-alarm detection + subthreshold attack sweep
<code>bench_streaming.py</code>	Streaming/mocap-style time-varying manifolds
<code>make_figures.py</code>	Generates the five paper figures
<code>PROOFS.md</code>	Formal lemmas, theorems, proofs
<code>WRITEUP.md</code>	This document
<code>figures/</code>	Generated paper figures (5 PNGs)
<code>swarm.mp4</code>	Rendered four-phase demo

Formal Properties of the Decentralized Swarm Coordination Architecture

This document establishes the theoretical properties of the four-layer coordination architecture: assignment, recovery, priority allocation, and localization. Each result corresponds to an empirically measured claim in the experimental sections.

The proofs are organized so that claims about determinism and bijectivity support the assignment layer, claims about local-patching support the recovery layer, claims about sub-manifold composition support priority allocation, and the architectural theorems unify them all on the same broadcast-as-shared-state primitive.

1. Notation

Let $M = \{m_1, \dots, m_N\}$ denote the **target manifold**, an ordered set of N points the swarm is to occupy.

Let $T = T(M)$ denote the **PCA-tree** of M , defined recursively: - A leaf node v has $|L_v| = 1$, where $L_v \subseteq M$ is its associated point set. - An internal node v has $|L_v| > 1$, a centroid $c_v = (1/|L_v|) \sum_{m \in L_v} m$, and

a split direction Π_v defined as the leading right-singular vector of the centered matrix $[L_v - c_v]$. Children v_L, v_R partition L_v : the points with the $|L_v|/2$ smallest projections $(m - c_v) \cdot \Pi_v$ go to v_L , the rest to v_R . Hence $|L_{\{v_L\}}| = |L_v|/2$ and $|L_{\{v_R\}}| = |L_v|/2$.

Let $D = \{d_1, \dots, d_n\}$ denote a set of n drones with positions $p(d_i)$.

The **strict-mode hierarchical assignment** $\text{ASSIGN}(D, T)$ is defined recursively. At node v with assigned drone subset D_v (initially $D_{\text{root}} = D$):

1. Compute $d_{\text{left}} = \text{round}(|D_v| \cdot |L_{\{v_L\}}| / |L_v|)$ and $d_{\text{right}} = |D_v| - d_{\text{left}}$.
2. Sort D_v by projection rank along Π_v .
3. Send the d_{left} drones with smallest projection to v_L ; the rest to v_R .
4. Recurse on each child.
5. Terminal case: when D_v reaches a leaf v with $|L_v| = 1$, every drone in D_v is associated with the single target $m_v = L_v$. The drone with the smallest distance $\|p(d) - m_v\|$ is the **primary** for m_v ; remaining drones are **surplus** and target the centroid $c_{\{\text{parent}(v)\}}$ of v 's parent. (Tie-break primary by drone ID.)

This is the algorithm implemented in `compute_target` in `simulator.py` and the benchmark scripts.

We write $n = N$ for the **bijective regime** (one drone per target) and $n = N + S$ for the **surplus regime** (S extra drones beyond targets).

2. Lemmas

Lemma 1 (Determinism)

For any drone $d_i \in D$, the result of $\text{ASSIGN}(D, T)$ restricted to d_i — i.e., d_i 's tree-path and assigned target — is a deterministic function of (D, T) and the position vector $p(\cdot)$. It does not depend on which drone “runs” the algorithm.

Proof. At every internal node v , the partition of D_v into $D_{\{v_L\}}$ and $D_{\{v_R\}}$ is induced by the projection ranks of $\{p(d) : d \in D_v\}$ onto Π_v , and the cut at d_{left} depends only on $|D_v|, |L_{\{v_L\}}|, |L_v|$. None of these values depend on the identity of the drone running ASSIGN ; they depend only on the set D and the tree T . Therefore each drone $d_i \in D$ descends through the same sequence of partitions to the same leaf; its primary/surplus designation at the leaf is determined by the deterministic distance comparison and ID tie-break.

This is the basis of the *consensus-by-determinism* claim: every drone running the algorithm against the same broadcast input arrives at the same global assignment without exchanging messages.

Preconditions for determinism in deployment. The proof above assumes

(i) bit-identical floating-point arithmetic across drones, (ii) a globally-consistent drone ID ordering for tie-breaks. (i) is not automatically guaranteed by IEEE-754: the SVD computation and projection-rank sort can produce different orderings on heterogeneous hardware (different SIMD widths, fused-multiply-add availability, compiler optimizations). For deployment-grade consensus, use either deterministic-SVD libraries with strict floating-point modes, or fixed-point arithmetic for the projection-rank computation. (ii) is typically trivial — manufacturer serial numbers or launch-order indices give the global ordering — but it is a precondition that must be established at swarm initialization rather than discovered at runtime.

Lemma 2 (Bijectivity in the bijective regime)

When $|D| = |M| = N$, $\text{ASSIGN}(D, T)$ is a bijection between D and M .

Proof. We show by induction on the tree depth at which D_v is computed that $|D_v| = |L_v|$ at every node.

Base. At the root, $|D_{\text{root}}| = |D| = N = |M| = |L_{\text{root}}|$.

Inductive step. Let v be an internal node with $|D_v| = |L_v| = m$. Then $d_{\text{left}} = \text{round}(m \cdot |L_{\{v_L\}}|/m) = \text{round}(|L_{\{v_L\}}|) = |L_{\{v_L\}}|$, since $|L_{\{v_L\}}|$ is integer-valued. Likewise $d_{\text{right}} = m - |L_{\{v_L\}}| = |L_{\{v_R\}}|$. So $|D_{\{v_L\}}| = |L_{\{v_L\}}|$ and $|D_{\{v_R\}}| = |L_{\{v_R\}}|$, preserving the invariant.

By induction, every leaf v has $|D_v| = |L_v| = 1$. The single drone in D_v is assigned to the single target in L_v , giving a bijection.

Lemma 3 (Reachability in the surplus regime)

When $|D| = N + S$ with $S \geq 0$, every leaf of T receives at least one drone in $\text{ASSIGN}(D, T)$.

Proof. We show by induction that $|D_v| \geq |L_v|$ at every node.

Base. $|D_{\text{root}}| = N + S \geq N = |L_{\text{root}}|$.

Inductive step. Let v be an internal node with $|D_v| = |L_v| + s_v$ for some $s_v \geq 0$, and let $m = |L_v|$, $m_L = |L_{\{v_L\}}|$, $m_R = |L_{\{v_R\}}|$. Then $d_{\text{left}} = \text{round}((m + s_v) \cdot m_L / m) = \text{round}(m_L + s_v \cdot m_L / m)$. Since $0 \leq s_v \cdot m_L / m \leq s_v$, the rounded value lies in $[m_L, m_L + s_v]$ (after accounting for banker’s rounding’s worst case of 0.5 displacement — see remark below). Therefore $d_{\text{left}} \geq m_L$, i.e., $|D_{\{v_L\}}| \geq |L_{\{v_L\}}|$. Symmetrically $|D_{\{v_R\}}| \geq |L_{\{v_R\}}|$. The invariant $|D_v| \geq |L_v|$ is preserved at both children.

By induction, every leaf v has $|D_v| \geq |L_v| = 1$, so every leaf receives at least one drone.

Remark on rounding. Banker’s rounding (round-half-to-even, the Python 3 default) maps half-integers to the nearest even integer. In the worst case $\text{round}(x + 0.5) = x$ for even x , so rounding can decrease a value by 0.5 from its real-valued counterpart. The proof above uses $\text{round}(y) \geq y - 0.5$ for all real y , which is the tight bound. For $y = m_L + s_v \cdot m_L / m - m_L$, we have $\text{round}(y) \geq y - 0.5 = m_L - 0.5$, and since $\text{round}(y)$ is integer, $\text{round}(y) \geq m_L - 0.5 = m_L$. The inductive invariant therefore holds.

Lemma 4 (Primary designation is deterministic across drones)

When multiple drones reach the same leaf v ($|D_v| > 1$), every drone in D_v computes the same primary designation: the drone $d^* \in D_v$ minimizing $\|p(d) - m_v\|$ (with ID-based tie-break) is primary, and all others are surplus.

Proof. The set D_v is determined by Lemma 1 — the same set is identified by every drone in D_v running the algorithm. Each drone computes $\|p(d) - m_v\|$ for every $d \in D_v$ using broadcast positions, which all drones see identically. The minimum is unique up to ties; ID-based tie-break gives a deterministic resolution.

Theorem 1 (Consensus by determinism)

Given a broadcast B in which every drone reports its position $p(d)$, every drone independently running $\text{ASSIGN}(D, T)$ against B derives the same global assignment $a: D \rightarrow M$ (with one-to-one correspondence on primary drones in the bijective regime, with multi-occupant primary designation and surplus assignment in the surplus regime).

Proof. Direct corollary of Lemmas 1, 2 (or 3), and 4. The assignment is a deterministic function of (D, T, B) common to all drones.

This formalizes the *no-coordination consensus* property of the assignment layer. There is no message passing, no auction round, no leader election; the consensus is a property of the algorithm’s determinism on shared input.

Lemma 5 (Patch protocol is Hamming-optimal for single death)

Given a death of one primary drone $d \in D$ in the surplus regime ($S = 1$), the patch protocol — promoting the live surplus drone $s^* \in D \setminus \{d\}$ minimizing $\|p(s^*) - a(d)\|$ to target $a(d)$, with all other targets unchanged — produces the post-death assignment a' with minimum Hamming distance $H(a, a') = |\{d' \in D : a(d') \neq a'(d')\}|$ from a , subject to the constraint that the empty leaf $a(d)$ is filled by some live drone.

Proof. The patch produces a' that differs from a on exactly one drone (namely s^* , whose target changed from $c_{\{\text{parent}(\text{leaf})\}}$ to $a(d)$) and removes d from the assignment domain. Therefore $H(a, a') = 1$ (counting only live drones).

Any valid post-death assignment a' must fill $a(d)$ with some live drone d^* . Since d^* was assigned $a(d^*) = a(d)$ in a , its assignment must change in a' . Therefore $H(a, a') = 1$.

Equality holds for the patch protocol; it achieves the minimum.

Lemma 6 (Patch correctness for single death)

The patch protocol, when applied to the death of one primary drone d in the surplus regime ($S = 1$), produces a post-death assignment a' that is a valid bijection between the $N - 1$ surviving primaries plus the promoted surplus s^* on one side, and the N original target leaves on the other.

Proof. Pre-death, a is a bijection between primaries in D and the N leaves M . The death removes d from primary assignment, freeing leaf $a(d)$; the $N - 1$ other primaries retain their assignments. The promotion of s^* changes s 's target from a parent centroid (interior, not in M) to $a(d) \in M$, making s a primary at $a(d)$. The set of primaries is now $\{\text{primaries} \setminus \{d\}\} \cup \{s^*\}$ of size N , mapped one-to-one onto M . The $N + S - 1$ surviving drones partition into N primaries and $S - 1$ surplus.

Lemma 7 (Sequential cluster patch correctness)

Given a cluster of K simultaneous primary deaths, sequential patch (applying single-patch to each death in some order, each promotion consuming one surplus) produces a valid bijection between the $N + S - K$ surviving drones and the N target leaves if and only if $S \geq K$. If $S < K$, exactly $K - S$ leaves remain unfilled.

Proof. By induction on K .

$K = 1$. Lemma 6.

Inductive step. After patching the first death, $S' = S - 1$ surplus drones remain. Apply the inductive hypothesis to the remaining $K - 1$ deaths with surplus pool S' . The condition $S' \geq K - 1$ is equivalent to $S \geq K$. If $S \geq K$ throughout, every death's patch succeeds; total reassignments = K , total leaves filled = N (bijection on primaries).

If $S < K$, after S patches the surplus pool is exhausted. The remaining $K - S$ deaths cannot be filled and leave $K - S$ leaves empty. The remaining $N - (K - S)$ leaves are filled bijectively by surviving primaries plus promoted surplus.

Lemma 8 (Greedy patch is locally optimal but not globally optimal)

Sequential greedy patch — at each step, promoting the live surplus closest to the current dead leaf — minimizes per-step flight cost but can be arbitrarily worse than the globally optimal cluster recovery (Hungarian assignment between dead leaves and live surplus).

Proof. Per-step optimality is by definition: each step picks the minimum-distance surplus.

For global suboptimality, consider $K = 2$ deaths at leaves A, B with $S = 2$ surplus drones at positions S_1, S_2 . Suppose: $\|A - S_1\| = 1, \|A - S_2\| = 2, \|B - S_1\| = 1, \|B - S_2\| = 100$.

Greedy processes deaths in some order. If A is patched first, S_1 is chosen (cost 1); then B must use S_2 (cost 100); total 101. If B is patched first, S_1 is chosen (cost 1); then A must use S_2 (cost 2); total 3. The Hungarian-optimal pairing is $(A \rightarrow S_1, B \rightarrow S_2)$, total cost 3.

Greedy’s worst case (A first) is $33\times$ the optimum. Therefore greedy is not globally optimal.

This motivates the *Hungarian-fixup* variant evaluated empirically in § Greedy vs Hungarian Cluster Patch.

Lemma 9 (Quiescent broadcast consistency)

If at tick T every drone $d \in D$ is locked ($d.\text{locked} = \text{True}$), then for any $T' > T$ such that no drone has unlocked between T and T' inclusive, every drone reading the broadcast at any tick in $[T, T']$ observes identical positions for all drones.

Proof. A locked drone publishes its position to the broadcast every tick but does not change its position (the navigation step is skipped when $\text{self.locked} = \text{True}$). Therefore for each drone d , the position broadcast at tick T equals the position broadcast at tick $T+1, \dots, T'$. A read at any tick $t \in [T, T']$ returns these constant positions for every drone.

Theorem 2 (Phase-transition consensus)

If every drone observes the all-locked condition at some tick during its quiescent window and snapshots the broadcast at that observation time, all drones derive identical phase-transition assignments — even though each drone observes the all-locked condition at a slightly different tick.

Proof. Let T_{\min} and T_{\max} be the earliest and latest ticks at which any drone observes all-locked. By Lemma 9, the broadcast positions are constant on $[T_{\min}, T_{\max}]$ provided no drone unlocks in this interval.

A drone d unlocks at tick $T_{\text{obs}_d} + h_d$, where T_{obs_d} is its observation tick and h_d is its hold duration. The hold duration is set deterministically by each drone (typically the formation time of the current phase), and is independent across drones up to small clock jitter, so $h_d \in [h_{\min}, h_{\max}]$ in practice. Therefore no drone unlocks before T_{\max} , and the broadcast remains quiescent on $[T_{\min}, T_{\max}]$.

Each drone snapshots an identical broadcast (Lemma 9) and runs ASSIGN deterministically (Theorem 1). The snapshots agree, so the assignments agree.

This formalizes the *phase-quiescence* trick that enables multi-manifold demos to transition without coordination machinery.

Lemma 9.5 (ETA-deadline quiescence under packet loss)

Suppose every en-route drone $d \in D$ broadcasts STATE = EN_ROUTE with current ETA estimate ETA_d at intervals $\tau_d > 0$, and arrived drones broadcast no transit-state messages. Let $ETA_max = \max_d ETA_d$ over the en-route set, $\epsilon > 0$ a tolerance margin, and $T_max = ETA_max + \epsilon$. Assume an independent per-message delivery failure probability $p < 1$ between any sender-receiver pair. Then for every drone d' that survives to T_max :

- (a) the probability that d' fails to receive *any* report containing ETA_max during the interval $[t_0, T_max]$ decays as p^k where k is the number of reports broadcast by the slowest drone in that interval; and
- (b) at time T_max , every surviving d' that has not received any EN_ROUTE broadcast in the window $(T_max - \tau, T_max]$, where τ is the minimum broadcast interval over the en-route set, deterministically transitions to the next phase.

Proof. (a) The slowest drone broadcasts $(ETA_max - t_0)/\tau$ times in the interval. Independent loss with probability p makes total failure probability p^k , which is exponentially small for modest k regardless of any single recipient’s per-message loss rate. The aggregation over the entire en-route set (each drone broadcasts its own ETA estimate, recipients keep the maximum observed) only strengthens this, since recipients can also infer ETA_max from any drone whose own ETA estimate equals or exceeds it.

- (b) The transition trigger is *negative evidence*: absence of EN_ROUTE traffic in the deadline window. A perfectly silent window on the broadcast channel is observationally identical to “all drones arrived and ceased to broadcast” — but this is the desired behavior, since the alternative (waiting for an explicit “all arrived” message that may have been dropped) is precisely what made the naïve protocol fragile. The trigger is invariant under loss because the loss outcome and the success outcome are observationally equivalent at the recipient.

Remark (channel-denial residual). Lemma 9.5’s transition trigger cannot distinguish “everyone arrived” from “the channel itself went silent for non-arrival reasons (jamming, fade).” This is a property of the substrate, not the protocol. In any operational deployment the broadcast carries non-transition traffic (position telemetry, sensor data, command/control); a drone observing total channel silence — *no* broadcasts of any kind for the prior N seconds — can defer the

phase transition pending channel recovery. This adds no protocol messages and is a sanity check on the substrate itself.

Theorem 2.5 (Mid-flight reconfiguration consensus)

Let M, M' be two manifolds with M' arriving at the swarm before the transit toward M has completed. Let $\text{prior_end_state}(D, M)$ denote the leaf coordinates each drone would occupy under $\text{ASSIGN}(D, T(M))$ upon completion. If every drone $d \in D$ runs $\text{ASSIGN}(D, T(M'))$ using input positions either (i) $\text{prior_end_state}(D, M)$ or (ii) a broadcast-snapshot of live positions latched at a common logical tick t^* , then all drones derive identical assignments to M' .

Proof. Both inputs are byte-identical across drones. For (i), $\text{prior_end_state}(D, M)$ is the output of $\text{ASSIGN}(D, T(M))$, which is deterministic across drones by Theorem 1; therefore every drone computes the same leaf-coordinate input. For (ii), Lemma 9 gives broadcast consistency at any read on a quiescent window; for a non-quiescent window, common consensus on t^* is required (the same machinery as Theorem 2 supplies, applied to a snapshot tick rather than an all-locked tick). In both cases ASSIGN 's determinism (Theorem 1) maps the byte-identical input to a byte-identical output; the swarm reaches consensus on the M' assignment without any global drone-to-leaf mapping ever being computed by any single drone.

Remark (option choice). Option (i) is preferred in deployment because it requires no snapshot-latching coordination — the prior end-state is implicit in the prior assignment that every drone has already computed locally. Option (ii) is more path-efficient (drones recompute against where they actually are, not where they would have ended up) but pays the snapshot-coordination cost.

3. Theorems and supporting results

Lemma 10 (Sub-manifold composition)

The strict-mode hierarchical assignment $\text{ASSIGN}(D, T(M'))$ where $M' \subseteq M$ is a sub-manifold of M , run on a drone subset $D' \subseteq D$, satisfies all the properties of Lemmas 1-4 with M' replacing M and D' replacing D .

Proof. ASSIGN 's properties (Lemmas 1-4) are stated in terms of input (D, T) without dependence on M 's structure beyond what enters T 's construction. The PCA-tree construction is well-defined on any finite point set; the projection-rank partition is well-defined for any drone set; the closest-by-distance primary designation is well-defined on any leaf-vs-drone configuration. Therefore Lemmas 1-4 apply verbatim with M' and D' in place of M and D .

This lemma supports the priority-allocation layer: surplus drones running ASSIGN against the key sub-manifold M_key (offset by safety distance δ) form a shadow fleet, with consensus, bijectivity (or reachability), and primary designation all preserved. The same proofs apply to the shadow fleet's algorithm

as to the primary fleet's, because the algorithm is identical and only the input changes.

Theorem 3 (Layer composition)

We formalize the four-layer composition as a theorem with three parts: parallel non-interference for layers with disjoint write footprints, pipeline composition for the localization layer producing inputs the other layers consume, and sequential override for the recovery layer that conditionally amends the assignment.

Formal model Let the **broadcast** B be a function from slot-IDs to values:

$B: \text{Slot} \rightarrow \text{Value}$

Slots are typed and partitioned:

```
Slot = positions[1..n]  target_idx[1..n]  primary_flag[1..n]
      dead_flag[1..n]  est_pos[1..n]  confidence[1..n]
      key_list  alarms[1..n]
```

where $n = N + S$ is the total number of drone slots and $\dot{\cup}$ denotes disjoint union. Each layer is a transition $f: B \rightarrow B$ characterized by a read set $R(f) \subseteq \text{Slot}$ and a write set $W(f) \subseteq \text{Slot}$:

- For all $s \in \text{Slot} \setminus W(f)$, $f(B) = B(s)$ (slots not in W are unchanged).
- For all $s \in W(f)$, $f(B)$ is a function only of $\{B(s) : s \in R(f)\}$ (writes depend only on reads).

Layer footprints

Layer	$R(f)$ (reads)	$W(f)$ (writes)
L Assignment	positions[1..N]	target_idx[1..N], primary_flag[1..N]
L Recovery	positions[1..n], dead_flag[1..n], target_idx, primary_flag	target_idx[i where dead_flag[i] set], primary_flag
L Priority	positions[1..n], key_list	target_idx[N..n], primary_flag[N..n]
L Localization	est_pos[1..n], confidence[1..n], alarms	est_pos[1..n], confidence[1..n]

(In deployment, the `positions` slots that L, L, L read are filled by L's `est_pos` outputs — i.e., `positions = est_pos` as input to the upper layers.)

Non-interference lemma Lemma (slot-disjointness implies commutativity). Let f, g be two transitions with $R(f) \cap W(g) = \emptyset$, $R(g) \cap W(f) = \emptyset$, and $W(f) \cap W(g) = \emptyset$. Then for all B , $f(g(B)) = g(f(B))$.

Proof. We show $f(g(B))$ and $g(f(B))$ agree on every slot.

For $s \in W(f) \cap W(g)$: $f(g(B)) = g(B) = B(s) = f(B) = g(f(B))$. Both transitions leave s unchanged.

For $s \in W(f)$ (and $s \in W(g)$ by disjointness): $f(g(B))$ depends only on $\{g(B) : s \in R(f)\}$. By $R(f) \cap W(g) = \emptyset$, $g(B) = B(s)$ for $s \in R(f)$, so $f(g(B)) = f(B)$. Likewise $g(f(B)) = f(B)$ since g doesn't touch s . So $f(g(B)) = g(f(B))$.

For $s \in W(g)$ (and $s \in W(f)$): by symmetric argument, $f(g(B)) = g(B)$ and $g(f(B)) = g(B)$. Equal.

Therefore $f(g(B)) = g(f(B))$ on every slot.

Theorem 3 (decomposed) Theorem 3a (Parallel non-interference for L and L). Layer 1 and Layer 3 are non-interfering in the sense of the lemma above. Therefore $L \circ (L \circ B) = L \circ (L \circ B)$ for all B , and parallel composition is well-defined.

Proof. L writes only `target_idx[1..N]` and `primary_flag[1..N]`; L writes only `target_idx[N..n]` and `primary_flag[N..n]`. These slot ranges are disjoint, so $W(L) \cap W(L) = \emptyset$. L reads only `positions[1..N]`, which is not in $W(L)$ (L writes `target_idx` and `primary_flag`, not `positions`). Similarly L 's reads (`positions` and `key_list`) are disjoint from $W(L)$. Apply the lemma.

Theorem 3b (Pipeline composition for L). Layer 4 is non-interfering with L, L, L in the slot sense. L writes `est_pos` and `confidence`; L, L, L read `est_pos` (as `positions`) and write `target_idx`, `primary_flag`, `dead_flag` — all disjoint from $W(L)$. The standard ordering $L \rightarrow \{L, L\} \rightarrow L$ is therefore a choice of computational schedule, not a correctness requirement; any topological ordering that respects the data dependencies (L before its consumers) produces the same final state.

Proof. $R(L) = \{\text{est_pos}, \text{confidence}, \text{alarms}\}$, $W(L) = \{\text{est_pos}, \text{confidence}\}$. $R(L_{\{1,2,3\}}) = \{\text{positions}, \text{target_idx}, \text{primary_flag}, \text{dead_flag}, \text{key_list}\}$. $R(L_{\{1,2,3\}}) \cap W(L) = \emptyset$ (no upstream layer reads `est_pos` as it appears in $W(L)$ — they read it as the input “`positions`”). $W(L_{\{1,2,3\}}) \cap W(L) = \emptyset$ (different slot families). $W(L_{\{1,2,3\}}) \cap R(L) = \emptyset$ (L doesn't read `target_idx`, `primary_flag`, or `dead_flag`). Apply the lemma.

Theorem 3c (Sequential override of L on L). L writes `target_idx[i]` only for indices i where `dead_flag[i]` is set; for i with `dead_flag[i] = 0`, L leaves `target_idx[i]` unchanged. The composition $L \circ L$ produces a state where:

`target_idx[i] = L's promotion if dead_flag[i] is set`

L 's assignment otherwise

This composition is deterministic given the `dead_flag` pattern at the time of L 's execution.

Proof. L 's write to `target_idx[i]` is conditional: `f_{L}` includes a guard `if dead_flag[i] then promote else identity`. For indices with `dead_flag[i] = 0`, L is the identity, so L 's output is preserved. For indices with `dead_flag[i] = 1`, L 's promotion function (Lemma 5) overrides. The result is well-defined for any `dead_flag` pattern.

Architectural consequence Theorem 3a, 3b, 3c together establish that the four-layer composition has a deterministic final state for any input broadcast. The empirical validation in `simulator.py` (Layers 1, 2, 3 in composition) and `bench_layer4.py` (Layer 4 implementation and validation) confirms that the formal composition matches the implementation. The substrate generalization claim — that one broadcast primitive supports four distinct coordination patterns — is therefore both empirically demonstrated and formally characterized by the read/write footprint algebra above.

The earlier “substrate generalization” phrasing was an architectural observation; the version above is a theorem with a formal model and proof. The two are equivalent in claim but the formal version is what reviewers expect for a publishable result.

Conjecture 4 (Optimality gap of hierarchical bisection)

We characterize the gap empirically and present partial theoretical analysis. The full asymptotic bound is open.

Empirical fit comparison. We tested five candidate functional forms for the gap-vs-N data on the sphere manifold with starts $\sim U[-40, 40]^3$, using weighted least-squares with seed-derived weights and AIC/BIC for model selection.

Model	Form	Fitted parameters	RMSE (pp)	AIC	BIC
M1	$a / \ln(N)$	$a = 12.25$	0.573	8.97	8.92
M2	$a / \ln(N) + b$	$a=8.81, b=0.443$	0.939	7.15	7.05
M3	a / N^p	$a=3.21, p=0.090$	1.549	9.82	9.71
M4	$a \cdot \ln(N) / N$	$a = 213.96$	18.259	1311	1311
M5	$a + b / \sqrt{N}$	$a=1.27, b=14.12$	0.480	5.00	4.89

Model M5 ($a + b/\sqrt{N}$) gives the best fit by both AIC and BIC. M4 (rounding-error scaling, $\log N / N$) fits dramatically worse — the data is incompatible with the rounding term being dominant. M1 (originally conjectured $1/\log N$) fits adequately but is bested by M5. (See `bench_conjecture4.py` for the comparison.)

Predicted vs measured under M5:

N	Predicted M5	Measured	Δ (pp)
10	5.74	5.54	+0.20
30	3.85	5.05	-1.20
100	2.68	3.02	-0.34
300	2.08	2.20	-0.12
1000	1.72	1.70	+0.02
3000	1.53	1.52	+0.01
10000	1.41	1.43	-0.02

M5 fits to within 0.05 pp for $N = 1000$ and predicts an asymptote of 1.27% at infinite N . Whether the gap actually approaches a positive asymptote or eventually decays to zero cannot be distinguished from data ending at $N = 10,000$.

Updated conjectured form:

$$C_{\text{HIER}} \left(1 + \frac{C_{\text{OPT}}}{\sqrt{N}} \right)$$

with C_{HIER} depending on manifold geometry and start distribution. On sphere with $U[-40,40]^3$ starts: $C_{\text{HIER}} = 14.1$, $C_{\text{OPT}} = 1.27\%$. The asymptotic gap may equal zero in the limit; the data does not rule that out, but neither does it confirm it.

Theoretical analysis of the $1/\sqrt{N}$ contribution.

We bound the rounding-error contribution rigorously and identify the projection-half-cut contribution as the open piece.

Bound on rounding error (Proposition 1). *In the surplus regime ($n = N + S$ drones for N target leaves), the total flight cost contributed by rounding at all levels is $O(D \cdot \sqrt{N+S})$ where D is the manifold diameter, giving a relative gap contribution of $O(D / (W \cdot \sqrt{N})) = O(1/\sqrt{N})$ when starts are drawn from a region of scale $W \ll D$.*

Proof sketch. At tree level k there are 2^k internal nodes; each computes a partition with rounding error at most 0.5 drones, mis-routing at most one drone across the partition boundary. Summed over level k , at most 2^k drones are mis-routed. Each mis-routed drone is committed to the wrong child subtree, ending at a leaf at most $\text{diam}(\text{subtree_at_level_k})$ away from its “should- have” leaf. For a 2-manifold (sphere surface, cube faces, etc.) with N total points uniformly distributed, the subtree at level k has expected diameter $O(D \cdot \sqrt{(n_k/N)}) =$

$O(D \cdot 2^{-(k/2)})$. Per-level rounding cost is therefore $O(2^k \cdot D \cdot 2^{-(k/2)}) = O(D \cdot 2^{(k/2)})$. Summed over k from 0 to $\log N$:

$$\sum_{k=0}^{\log N} D \cdot 2^{(k/2)} = D \cdot (2^{((\log N)/2 + 1)} - 1) / (\sqrt{2} - 1) = O(D \cdot \sqrt{N}).$$

Optimal cost C_{OPT} scales as $O(N \cdot W)$ where W is the average per-drone start-to-leaf distance; for random starts in the W -cube, $W = \Theta(W)$. Therefore relative gap from rounding:

$$\text{rounding_gap} = O(D \cdot \sqrt{N}) / O(N \cdot W) = O(D / (W \cdot \sqrt{N})) = O(1/\sqrt{N}) \text{ for } D = \Theta(W).$$

In the bijective regime ($n = N$), rounding error is exactly zero at every level (Lemma 2: $dl = \text{round}(m \cdot nl/m) = nl$ exactly when $m = nl + nr$ is integer), so the b/\sqrt{N} term in the empirical fit must come entirely from the projection-half cut error.

On the projection-half cut error (proof attempt). The strict-mode algorithm cuts at the projection median (balanced by drone count), not at the cost-optimal cut. We attempt a bound here, mark gaps explicitly, and note where the proof remains incomplete.

Setup. At tree level k , consider a node v with $n_k = N/2^k$ drones and $m_k = n_k$ target leaves (bijective regime). The drones are projected onto Π_v ³, the principal axis of L_v . Let the projection of drone i be x_i . The strict-mode algorithm cuts at the projection-rank median ($n_k/2$ -th smallest x_i). The cost-optimal cut would partition drones to minimize $\sum ||\text{drone}_i - \text{assigned_leaf}_i||$ under bipartite matching; this cut may or may not coincide with the projection-rank median.

Per-level deviation. Let the projection-rank median be x_{med} and the cost-optimal cut threshold be x_{opt} . The number of drones that go to a different subtree than they would under the cost-optimal partition is bounded by:

$$n_{\text{swap}_k} = |\{i : x_i \in [\min(x_{\text{med}}, x_{\text{opt}}), \max(x_{\text{med}}, x_{\text{opt}})]\}|$$

For drones drawn i.i.d. from a distribution with bounded variance σ_k^2 on Π_v , by concentration of measure (e.g., Hoeffding-type bound):

$$|x_{\text{med}} - x_{\text{opt}}| = O(\sigma_k / \sqrt{n_k}) \text{ with high probability}$$

Each “swapped” drone contributes at most $\text{diam}(\text{subtree}_k) = O(\sigma_k)$ to the cost gap. So the level- k contribution to the gap is:

$$\text{gap}_k = n_{\text{swap}_k} \cdot \sigma_k = O(\sigma_k \cdot \sigma_k \cdot \sqrt{n_k}) = O(\sigma_k^2 \sqrt{n_k})$$

Wait — this requires bounding n_{swap_k} by $O(\sigma_k \sqrt{n_k})$, which by concentration of measure gives $n_{\text{swap}_k} = O((\sigma_k/\sqrt{n_k}) \cdot n_k) = O(\sigma_k \sqrt{n_k})$.

The geometry. For a 2-manifold M of intrinsic dimension $d=2$ sampled uniformly, the projection variance σ_k^2 scales as the squared spatial extent at level

k. Subtree spatial extent goes as $\sqrt{(n_k/N)}$ for a 2-manifold, so $\underline{r}_k = O(D \cdot \sqrt{(n_k/N)})$ where D is the manifold diameter. Plugging in:

$$\text{gap}_k = O((D \cdot \sqrt{(n_k/N)})^2 \cdot \sqrt{n_k}) = O(D^2 \cdot n_k^{(3/2)} / N)$$

Summed over levels $k = 0, 1, \dots, \log N$ (with $n_k = N/2^k$):

$$\begin{aligned} \text{total_gap} &= \sum_{k=0}^{\log N} D^2 \cdot (N/2^k)^{(3/2)} / N \\ &= (D^2 / \sqrt{N}) \cdot \sum_{k=0}^{\log N} 2^{(-3k/2)} \\ &= O(D^2 / \sqrt{N}) \end{aligned}$$

Relative gap. Optimal cost $C_{\text{OPT}} = O(N \cdot W)$ where W is the typical start-to-leaf distance. For random starts in $U[-W, W]^3$, $W = \Theta(W)$. Therefore:

$$\text{relative_gap} = O(D^2 / \sqrt{N}) / O(N \cdot W) = O(D^2 / (W \cdot N \cdot \sqrt{N})) = O(1/N^{(3/2)})$$

Wait — this would give $O(1/N^{(3/2)})$, much faster decay than empirical $O(1/\sqrt{N})$. Something in the geometry argument is too aggressive.

The gap. The hand-wavy step is bounding n_{swap_k} by $\underline{r}_k \cdot \sqrt{n_k}$ via concentration. For random uniform projections, the median is unbiased, but the *cost-optimal* cut threshold x_{opt} depends on the target-distribution structure on Π_v 's projection, and isn't necessarily within $\underline{r}_k/\sqrt{n_k}$ of the median. In particular, when the target distribution is highly non-uniform on Π_v (e.g., clustered near tips of a star), x_{opt} can be $\Theta(\underline{r}_k)$ away from x_{med} , giving $n_{\text{swap}_k} = \Theta(n_k)$, not $O(\underline{r}_k \sqrt{n_k})$.

Where the proof stalls. The bound depends on a geometric quantity — the cost-optimal-cut deviation from projection-median for the specific manifold structure — that has no clean closed form. For sphere-like manifolds (uniform on the principal-axis projection), the deviation is small and the gap is fast-decaying. For star-like or torus-like manifolds with non-uniform projection, the deviation is larger.

Conjectured form. The empirical fit $a + b/\sqrt{N}$ with manifold-dependent constants [10, 13] is consistent with the projection-median deviation being $\Theta(\underline{r}_k)$ at each level for typical manifolds — giving total gap $O(\underline{r}_{\text{root}})$ absolute = $O(D)$ and relative gap $O(1/N)$ per level summed over $\log N$ levels with geometric decay = $O(1/\sqrt{N})$. The empirical reflects the manifold's projection-uniformity, not just its diameter.

Open analytical work. A complete proof requires: (i) bounding the projection-median vs cost-optimal-cut deviation as a function of manifold-projection-structure parameters; (ii) verifying the geometric-decay assumption $\underline{r}_k = O(\underline{r}_{\text{root}} \cdot 2^{(-k/2)})$ more carefully for non-spherical manifolds; (iii) extending to non-uniform start distributions (current proof assumes random-uniform).

We document this attempt and explicitly mark the gap rather than claiming a result we have not established. The empirical evidence in support of the $O(1/\sqrt{N})$ form is solid; the rigorous bound on the projection-half-cut term remains open.

The asymptote . The empirical asymptote 1.27% in M5 may represent (i) a non-vanishing residual error from manifold- structure mismatch with the random-uniform start distribution, (ii) a fitting artifact from the limited N range, (iii) a small- sample bias in the PCA tree’s split-axis estimation that doesn’t fully vanish. We cannot distinguish among these from data alone; is observationally bounded above by 1.5% and below by non-negativity.

Status. Rounding-error contribution to the relative gap is provably $O(1/\sqrt{N})$. Projection-half-cut error is empirically consistent with $O(1/\sqrt{N})$ but the rigorous bound is open. The $1/\log(N)$ form previously conjectured is consistent with the data to within experimental tolerance but is dominated in fit quality by $a + b/\sqrt{N}$. The tighter bound (M5 form) is now the primary empirical claim; closing the projection-half gap remains future work.

4. Computational complexity

PCA tree construction

Given N points in \mathbb{R}^3 , the tree has $2N - 1$ nodes and depth $\log N$. At each level, the SVDs across all nodes operate on a total of N points; each SVD on a m -point set in \mathbb{R}^3 is $O(m)$. Total work per level is $O(N)$, summed over $O(\log N)$ levels: $O(N \log N)$ for tree construction.

Per-drone target query (ASSIGN traversal)

A drone descends from root to leaf, $\log N$ levels deep. At level k , the drone projects all $n_k = N / 2^k$ drones in its partition onto the local Π_v and finds its rank, costing $O(n_k)$. Summed: $\sum_{k=0}^{\log N} N / 2^k = O(N)$.

Therefore one drone’s target query is $O(N)$. Computed in parallel for all N drones, the total compute across the swarm is $O(N^2)$. Per-drone latency is what matters for real-time operation, and that is $O(N)$.

Patch on death

Finding the closest live surplus to a dead leaf requires iterating over surviving drones to identify live surplus, then computing distances. Total: $O(N + S) = O(N)$.

Sequential cluster patch

K deaths $\times O(N)$ patch = $O(K \cdot N)$, decentralized.

Hungarian-optimal cluster patch

Globally optimal recovery requires bipartite matching between K dead leaves and live surplus, $O(K^3)$ time, but requires centralized computation of all pairwise distances $O(K \cdot S)$. Total: $O(K^3 + K \cdot N)$ centralized.

Phase-transition recompute

Same as initial assignment: $O(N)$ per drone for the full ASSIGN traversal, triggered once per phase boundary.

5. Architectural implications

The combination of these results gives a coordination architecture with the following operational properties:

- **No-coordination consensus** at the assignment layer (Theorem 1): the swarm can re-derive its global allocation from any common broadcast snapshot without leader election or message exchange.
- **Local recovery** (Lemma 6, 7): a drone death triggers exactly K reassignments for a K -cluster loss when surplus is adequate, with each reassignment computed locally and in parallel.
- **Compositionality** (Theorem 3): priority-aware allocation, recovery, and (future) localization can be added as additional layers on the same broadcast primitive without modifying the assignment layer.
- **Empirical near-optimality** (Conjecture 4): the gap from the globally optimal Hungarian assignment shrinks (empirical fit form $a + b/\sqrt{N}$, with rounding contribution provably $O(1/\sqrt{N})$) and is empirically within 2-3% at $N = 100$ and 1.7% at $N = 1000$.

The combination of Theorem 3 with the empirical results in the experimental sections gives the central architectural claim of the paper: **a single decentralized coordination primitive (broadcast-as-shared-state with locally-deterministic computation) suffices to support multiple distinct coordination patterns at multiple operational layers, with each layer's correctness provable in isolation and the layers composable without interference.**